THESIS APPROVAL

The abstract and thesis of Peter James Sniffen for the Master of Science in Geology: Geohydrology were presented July 30, 2007, and accepted by the thesis committee and the department.

COMMITTEE APPROVALS:

_____
Andrew G. Fountain, Chair

_____
Kenneth M. Cruikshank

_____
Christina L. Hulbe

_____
John G. Rueter
Representative of the Office of Graduate Studies

DEPARTMENT APPROVAL:

_____
Michael L. Cummings, Chair
Department of Geology

ABSTRACT

An abstract of the thesis of Peter James Sniffen for the Master of Science in Geology: Geohydrology presented July 30, 2007.

Title: Dry calving at the terminus of a polar glacier, Taylor Glacier, McMurdo Dry Valleys, Antarctica.

The polar glaciers of the McMurdo Dry Valleys, Antarctica terminate on dry land yet exhibit terminal morphologies characterized by near-vertical cliffs that are partially maintained by the process of dry calving. Ice flow data collected between 2003 and 2007 on Taylor Glacier are described and illuminate some of the processes that contribute to the development of the near-vertical ice cliffs.

Surface velocities are higher in the interior of the glacier (5.0 ± 0.14 ma^{-1}) and lower along the sides (3.0 ± 0.14 ma^{-1}). At surface sites located within 20 meters of the cliff, velocity in the cliff-parallel direction increases with distance from the cliff while cliff-perpendicular velocities do not change appreciably. This motion is consistent with a strain regime of simple shear. Mapping of ice structures at the near-cliff sites document fractures oblique to the cliff edge that are consistent with shearing. Strain rates on the order of 10^{-3} a^{-1} also indicate shear but uncertainty is also 10^{-3} a^{-1}.

The velocity profile of ice cliff face may contribute to an overhanging cliff profile. Ablation on the cliff face may contribute to undercutting more than ice flow.

Ablation ranges from 40 cm at the top of the cliff to over 100 cm near the base over the two-month summer season. Undercutting of the cliff face may create an unstable cliff. Fractures created by shearing at the surface may serve as planes of weakness and preferentially accommodate strain from the overhanging cliff face leading to calving events that return the cliff to a more stable vertical or sub-vertical profile.

DRY CALVING AT THE TERMINUS OF A POLAR GLACIER, TAYLOR GLACIER, MCMURDO DRY VALLEYS, ANTARCTICA

by

PETER JAMES SNIFFEN

A thesis submitted in partial fulfillment of the
requirements for the degree of

MASTER OF SCIENCE
in
GEOLOGY: GEOHYDROLOGY

Portland State University
2008

Table of Contents

List of Tables ii
List of Figures iii
Chapter 1: Introduction 1
1.1: Study Area 2
1.2: Calving Processes 5
1.3: Polar Ice Cliffs 8
Chapter 2: Methods 14
2.1: Surface Site Networks 14
2.2: Vertical Cliff Networks 19
Chapter 3: Results 21
3.1: Field Results 21
3.2: Surface Velocity 24
Chapter 4: Analysis 31
4.1: Strain Rate 33
4.2: Fracture Surveys 44
4.3: Vertical Cliff Sites 48
Chapter 5: Conclusion 56
Future Work 57
References 58

List of Tables

Table 1: Table of strain rate values and strain axes calculated for two seasons at Site 1. Winter values are shaded in the table. Quadrangle number refers to Figure 24. 36
Table 2: Table of strain rate values and strain axes calculated for two seasons at Site 2. Quadrangle number refers to Figure 24. 38
Table 3: Table of strain rate values and strain axes calculated for three seasons at Site 3. Winter values are shaded in the table. Quadrangle number refers to Figure 24. 41
Table 4: Velocities at Cliff Sites 1 and 2 for summer 2004-2005 and winter 2005. ... 48

List of Figures

Figure 1: Location of the McMurdo Dry Valleys, Antarctica. Approximately 77°N, 162°E. 3
Figure 2: Location of study site in the lower ablation area of Taylor Glacier in Taylor Valley. 4
Figure 3: Physical models of calving: thermal erosion below the water line (left) and physical erosion notch-cutting at the waterline (right). Both situations explain calving as a result of undercutting of the ice cliff. 6
Figure 4: Schematic diagram of bending shear. Note shear decreases with depth. Adapted from (Hughes, 1989a). 7
Figure 5: Bending shear in a grounded tidewater glacier (left) and a glacier at floatation (right) showing down warping of the terminus. From(Hughes and Fastook, 1997). 8
Figure 6: The grounding of the upper semi-rigid, and outer rigid rheological zones result in an impedance to flow and lead to the development of an ice cliff (Chinn, 1985; Holdsworth, 1969). From (Chinn, 1985). 10
Figure 7: The progression from ramped margin to cliffed margin is a result of the grounding of the upper semi-rigid zone and increased basal shearing and ramping of the glacier ice. From (Chinn, 1991). 11
Figure 8: Stages of marginal fold development leading from a ramped terminus (a) to a terminus with a vertical cliff (e). From (Chinn, 1989). 12
Figure 9: General layout of the two types of arrays used to measure ice flow on the glacier surface and the vertical ice cliff. 15
Figure 10: Field site locations on Taylor glacier. Circles represent clusters of 13 stakes and triangles represent individual stakes in a linear transect. 17
Figure 11: The layout of the cliff sites along the northern cliff of Taylor Glacier. The stake numbering conventions for all sites are the same as in Figure 12 below. 18
Figure 12: The layout of stakes at Site 3 in the interior of the glacier. 19
Figure 13: UNAVCO NZAP Benchmark TP1 (triangle) located at 77 43 10.4851 S 162 16 27.985 E in relation to project field site locations. 22
Figure 14: Velocity values during the summer of 2004-2005 for each site in the lower ablation zone of Taylor Glacier. Each triangle and associated velocity represents the average of 13 stakes in that area. Velocity vectors are scaled 40 times and reflect values between 5.0 and 3.0 ma^{-1}. 25
Figure 15: Velocity vectors at Site 3 laid tip to tail for three seasons of study. Note consistent direction and only a slight increase in magnitude throughout the duration of the study. 26
Figure 16: Velocities at Site 1 and Site 2. Site 2 velocities are slightly higher than at Site 1 but there is no significant difference between winter and summer velocities at each site. 27
Figure 17: Downstream velocities at Site 1 and 2 show increasing velocity with distance from the cliff for both Summer and Winter seasons. 28

Figure 18: Cliffward velocities at Site 1 and Site 2 show weak trends of decreasing velocity with distance from the cliff for both summer and winter seasons. 28
Figure 19: Velocity vectors for three seasons at Site 1 plotted head to tail in chronological order. There is little change during the first two seasons (blue and green arrows), however the motion of stakes 2 and 12 (labeled) changes dramatically during the second summer (red arrows). 30
Figure 20: Velocity vectors for three seasons at Site 2 (Perfection) plotted head to tail in chronological order. Note the dramatic change in velocity for stakes 2, 6, and 11 (labeled) that occurred during the summer season of 2005-06 (red arrows)... 30
Figure 21: A pattern of increasing downstream velocity with distance from the cliff edge indicates a stress regime consistent with simple shear. Dotted line represents a square deformed through left-lateral shear consistent with observed stake motion. 31
Figure 22: Diagram showing generalized strain quadrangle. Capital letters and solid circles represent the original position of stakes while lower case open circles are final positions. The dotted square represents the area for which strain is calculated. Because we use average velocities, the strain is calculated at the average stake position. 34
Figure 23: Schematic of non-overlapping quadrangles used for strain rate calculations at Site 1 and Site 3 (left) and Site 2 (right). The quadrangles are numbered for future reference. Site 3 was arranged identically to site 1b. 36
Figure 24: Principle strain rates calculated at Site 1 for summer of 2004-2005 (upper graph) and winter 2005 (lower graph) seasons. Red lines indicate extensional strain while blue represents compressional strain. The strain ellipses are scaled by $x10^{-3}$ a^{-1}. 37
Figure 25: Principle strain rates calculated at Site 2 for the summer of 2004-2005 (upper graph) and winter 2005 (lower graph) seasons. Red lines indicate extensional strain while blue represents compressional strain. The strain ellipses are scaled by $1x10^{3}$ a^{-1}. 39
Figure 26: Principle strain rates calculated at Site 3 for the summer of 2004-2005. The anomalously high strain rates during this measurement period are attributed to the shifting of stakes as they refroze after initial measurement. The strain ellipses are scaled by $1x10^{3}$ a^{-1}. 40
Figure 27: Principle strain rates calculated at Site 3 for the summer of 2005-2006 (upper graph) and winter 2005 (lower graph) seasons. Red lines indicate extensional strain while blue represents compressional strain. The strain ellipses are scaled by $1x10^{3}$ a^{-1}. 42
Figure 28: Surface Site 1 2004-2005 season. Based on field sketch and measurements taken by Peter Sniffen. 46
Figure 29: Surface Site 1 2005-2006 season. Dashed circles represent stakes lost to melt-out or calving. Based from field sketch and measurements taken by Matt Hoffman 46
Figure 30: Fracture map of Surface Site 2, 2004-2005 season. From field sketch and measurements by Peter Sniffen. 47

Figure 31: Fracture map of surface Site 2 from the 2005-2006 season. From field sketch and measurements collected by Matt Hoffman. 47
Figure 32: Cliff-parallel and cliff-perpendicular velocities measured at Cliff Site 2 during Summer 2004-2005. 49
Figure 33: Cliff-parallel and cliff-perpendicular velocities measured at Cliff Site 2 during winter 2005. 50
Figure 34: Velocities measured at Cliff Site 1 for the summer of 2004-2005. 51
Figure 35: Winter 2005 velocities measured at Cliff Site 1 51
Figure 36: Ablation for both cliff sites for summer of 2004-2005 (top) and winter 2005 (bottom). Values for Cliff Site 1 are represented by hollow bars. Both sites lost stakes over the winter season. 53
Figure 37: Cliff profile change at Cliff Site 2 showing summer, winter, and total year profile change. 54

Chapter 1: Introduction

Calving is the mechanical fracturing and failure of glacier termini and can be an important ablative process (Van der Veen, 1996). For glaciers that terminate in water, calving results in icebergs. Generally speaking there are two modes of calving. One is the calving of large tabular icebergs from floating ice shelves, which produce huge icebergs on the order of 10^3 km^2. The second mode is the calving of grounded "tidewater" glaciers, which tend to produce much smaller icebergs ($\leq$100 m^2) (Benn and Evans, 1998). Calving is a particularly large component of ablation in tidewater glacier systems (Meier, 1997). As a result, research on calving dynamics has been largely focused on these glaciers. Past studies have relied on photogrametry and aerial photography as large parts of their data sets (Kirkebride and Warren, 1997).

The calving process of tidewater glaciers is still not well understood. The high flow velocities, large height of terminal cliffs, and frequent calving makes them difficult to study. Instrumentation of the cliffs is dangerous or impossible in many situations and studies are limited to indirect measurements correlating calving rate, flow velocity, water depth, ground slope, etc. (Hanson and Hooke, 2000; Hughes, 1989a; Kirkebride and Warren, 1997; Paterson, 1994; Van der Veen, 1996). Correlations exist between calving rate and water depth at the terminus, however other factors such as longitudinal strain rate and temperature also play a role in determining calving rates. Studies limited to indirect measurements of calving rate make it difficult to partition factors like temperature and strain rate, and the causal relationship remains elusive (Hanson and Hooke, 2000; Van der Veen, 2002). Examining calving

processes for a grounded polar glacier will allow us to look at factors such as temperature and longitudinal strain rate separate from water depth. This will help identify what role these other factors play in terminus stability and can be applied to the dynamics of tidewater calving.

The aim of this project is to conduct a detailed study of the dynamic processes acting at the terminus of a grounded polar glacier. Small alpine glaciers in the Taylor Valley of Antarctica terminate on dry land and exhibit vertical cliffs that are maintained partially by periodic calving events through a process known as dry calving. I analyze the ice flow dynamics at two near-terminus sites and one interior site on Taylor Glacier, Antarctica to investigate the role of ice-flow in dry calving.

1.1: Study Area

Taylor Glacier is an outlet glacier of the East Antarctic Ice Sheet and flows into Taylor Valley, one of the McMurdo Dry Valleys, Antarctica (Figure 2), 77° S, 162°E. Taylor Valley is oriented east-west and is approximately 35 km long, bounded by the Kukri Hills to the south and the Asgard Range to the north and filled by Taylor Glacier at the western end. Many small alpine glaciers flow into the Taylor Valley from the mountains bordering the valley. Three perennially ice-covered lakes (Lakes Bonney, Hoare, and Fryxell) are located within the Taylor Valley fed by ephemeral streams that drain melt from the glaciers. Average temperatures in the Taylor Valley range between -16 and -21°C (Doran et al., 2002). The summer season lasts for approximately 10 weeks between November and January and is characterized by temperatures that fluctuate around 0°C. Winter temperatures reach lows of -60°C and

are influenced by strong katabatic winds from the Antarctic Plateau (Nylen et al., 2004). Annual precipitation averages less than 10 cma^{-1} making the dry valleys region a polar desert (Doran et al., 2002).

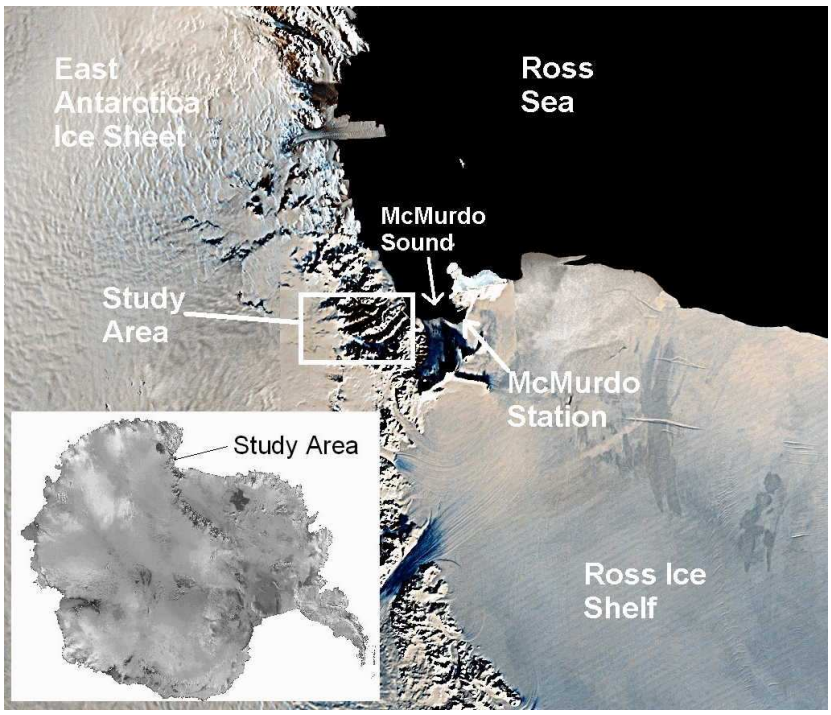

Figure 1: Location of the McMurdo Dry Valleys, Antarctica. Approximately 77°N, 162°E.

Taylor Glacier is approximately 100 km long from its origins at Taylor Dome and partially terminates in Lake Bonney (Robinson, 1984). We focus on the lower ablation area within 1 km of the terminus. In the lower ablation area the mean annual surface temperature of Taylor Glacier in the lower ablation area is -17°C (Nylen, 2004, Robinson, 1984). Average surface flow velocity varies with location from 4.5 ma^{-1} and 7.5 ma^{-1} (Johnston, 2004). Possibly 50% of the lower glacier may be melting at the base.

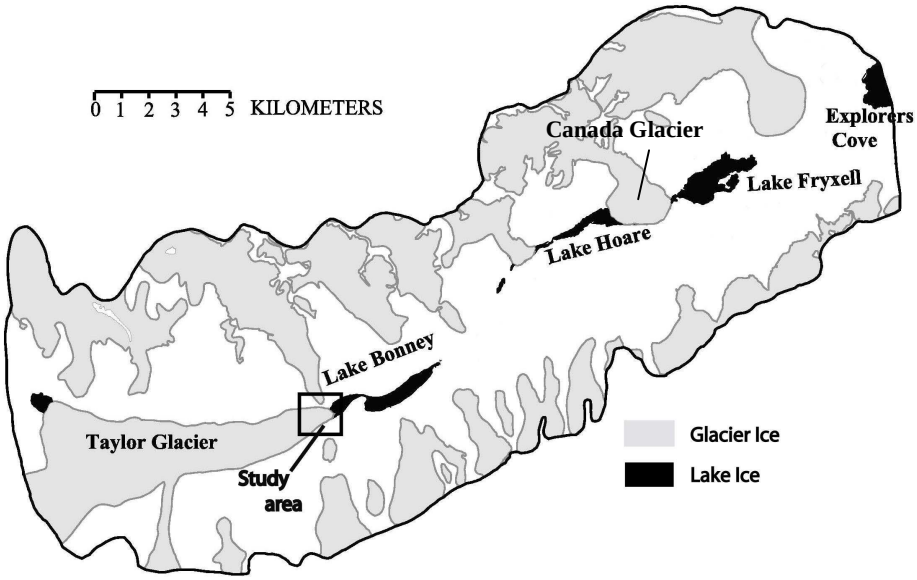

Figure 2: Location of study site in the lower ablation area of Taylor Glacier in Taylor Valley.

Processes at glacier termini affect the mass balance of a glacier. Glacier ablation occurs by melt, evaporation, sublimation, and calving. On Canada Glacier (Figure 2), the terminal cliffs constitute only 2% of the total ablation area but they account for 15-20% of the melt runoff (Fountain et al., 1999). Calving plays a role in ablation by physical removal of ice and by shaping the morphology of the terminus. Solar radiation on a vertical cliff in the polar region makes an angle closer to normal than on the sub-horizontal glacier surface (Chinn, 1987; Fountain et al., 1999). The more intense solar radiation and long-wave radiation from the valley floor, increases melt on the cliffs. Also, calving piles ice on the warm valley floor, aiding meltwater production.

1.2: Calving Processes

Several theories have been proposed to explain concerning the mechanism driving calving. Most have been in relation to tidewater calving and identify undercutting of the cliff face as primary in the calving mechanism (Hanson and Hooke, 2000; Hughes, 1989a; Kirkebride and Warren, 1997; Van der Veen, 1996). The most widely accepted theories relate calving rate to water depth due to factors such as wave-action undercutting, submarine melting, or buoyant forcings (Hanson and Hooke, 2000; Kirkebride and Warren, 1997). Other theories link the calving mechanism to the internal flow regime and structure of the ice (Hughes and Fastook, 1997). These theories have been criticized with the suggestion that they only describe codependent mechanisms while leaving the true driving mechanism of calving undiscovered (Van der Veen, 2002).

At Maud Glacier, a New Zealand temperate glacier terminating in a lacustrine environment, calving was observed to occur in a four step process: 1) the cliff was undercut due to thermal erosion at the waterline; 2) the calving of small flakes increased the overhang at the waterline; 3) relatively infrequent calving events occurred as the result of collapse above the undercut cliff; and 4) rare calving events occurred from the sub aqueous ice cliff (Figure 3). The calving at Maud Glacier was attributed to the collapse of the ice cliff due to gravity as it was undercut at the waterline (Kirkebride and Warren, 1997).

Hanson and Hooke (2000) examined the physical mechanism behind the widely accepted empirical evidence suggesting the calving rate of tidewater glaciers is

directly proportional water depth at the terminus. Their results indicate calving rate does increase with water depth at the terminus, which they attribute to the development of an overhanging ice cliff. Modelling demonstrates that the distribution of longitudinal stresses and ice velocity near the terminus lead to the undercutting of the cliff face (Hanson and Hooke, 2000). Numerical models also indicate that submarine melting and basal drag both contribute to the overhanging cliff profile. While confirming water depth and calving rate are proportional, the relationship is not necessarily causal, and water depth is most likely just one of the variables controlling the calving rate (Hanson and Hooke, 2000).

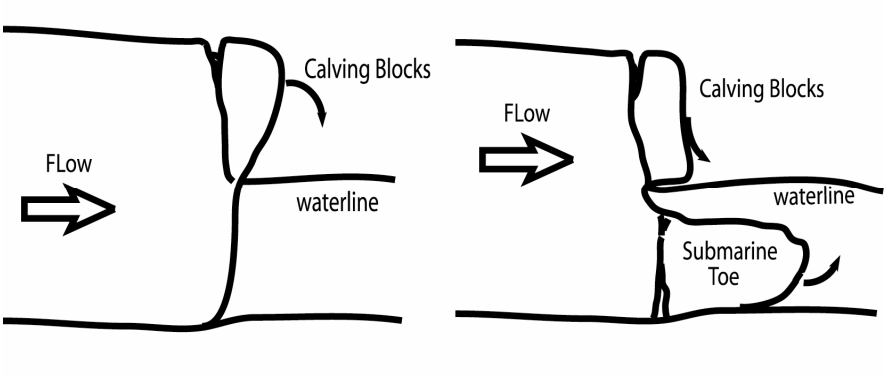

Figure 3: Physical models of calving: thermal erosion below the water line (left) and physical erosion notch-cutting at the waterline (right). Both situations explain calving as a result of undercutting of the ice cliff.

In a different interpretation of calving mechanics, Hughes (1989b) developed a model based on dry calving occurring on Deception Island, Antarctica. Shear bands were observed crosscutting ash layers in the ice, demonstrating motion is being accommodated in distinct vertical bands (Hughes, 1989b). This mechanism is compared to bending a book around its binding (Figure 4). The shear between the

zones is small near the bed (theoretically approaching zero) and increases towards the surface of the glacier. Bending shear continues until there is rupture along one of the shear zones. On Deception Island this was observed to occur when the ice wall of a grounded tidewater glacier reached an overhang of approximately 20° from vertical (Hughes, 1989b). Further examination of shear fabric formation revealed that recrystalization of ice crystals within the shear bands forms an "easy-glide fabric" that encourages rapid deformation along the shear zones (Hughes, 1989a). This rapid deformation ultimately leads to fracture and calving along the shear zones (Hughes, 1989a).

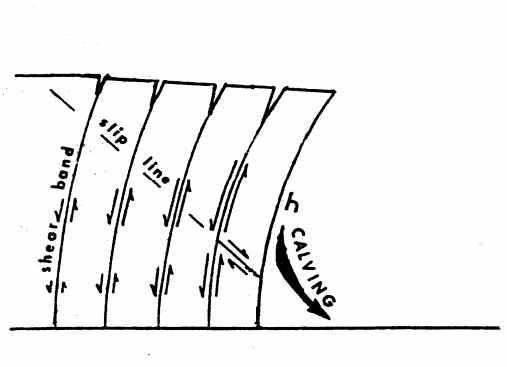

Figure 4: Schematic diagram of bending shear. Note shear decreases with depth. Adapted from (Hughes, 1989a).

The bending shear model requires significant basal shear stress, which is present in grounded glaciers, and especially polar glaciers that are frozen to their beds, but diminishes to zero as the glacier nears flotation. Tidewater glaciers experience significant basal shear stress if the water depth is insufficient to provide flotation. In systems where the water is deep enough, Hughes and Fastook (1997) suggest down-

warping of the glacier snout and the deposition of a terminal moraine may provide the necessary basal shear stress to initiate bending shear (Figure 5).

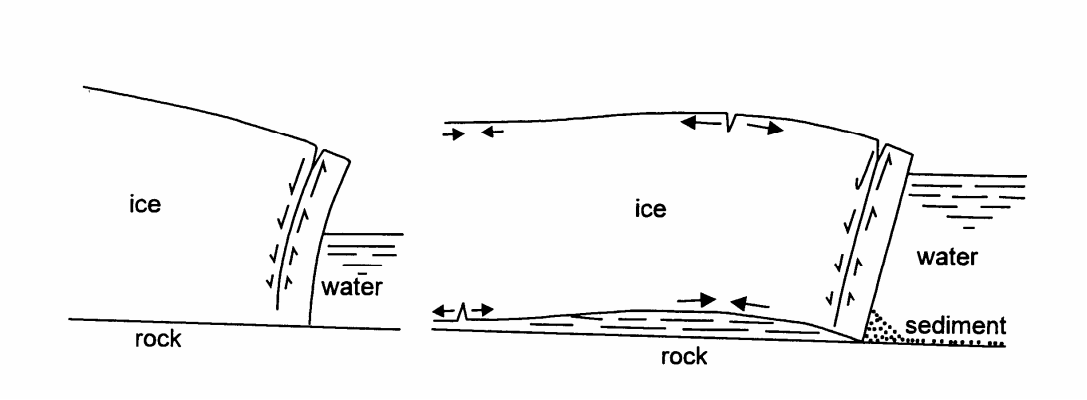

Figure 5: Bending shear in a grounded tidewater glacier (left) and a glacier at floatation (right) showing down warping of the terminus. From(Hughes and Fastook, 1997).

The conceptual models outlined above should not be thought of as mutually exclusive. Each model leads to some degree of an overhanging cliff face and ultimately failure and calving. Depending on the specific glacial system, any of these models may be working alone or simultaneously to contribute to the ultimate failure of the cliff. But Van der Veen (2002) asks the question: do any of these models really address the driving forces behind calving or are they just describing coincidental empirical relationships? He suggests a causal relationship between glacier geometry and dynamics, specifically ice speed and thickness as the factors controlling calving rate (Van der Veen, 2002).

1.3: Polar Ice Cliffs

Cold-based glaciers have been observed to terminate in 20-30 meter ice cliffs in polar regions and high altitude regions such as Mt Killimanjaro, Northern Greenland, and Antarctica (Van der Veen, 1997). The uniformity of the cliffs in these

regions has led to research into how ice cliffs form and why their geometry is so similar across different regions.

Previous work suggests ice cliffs form as a result of a combination of rheological changes in the ice, macro-scale structural deformation, and changes in mass balance due to cliff-generated microclimates. Holdsworth (1969) describes four rheological zones in the tongue of the polar glacier (Figure 6). Based on a perfectly plastic model, the ice cliffs exist as a result of an upper semi-rigid zone that becomes grounded as the glacier thins to the terminus (Chinn, 1985; Holdsworth, 1969). The glacier is described as consisting of a rigid surface shell riding on a "plastic glacier"(Chinn, 1985).

Most, if not all, of the glaciers in the McMurdo Dry Valleys have a basal ice layer that has a high chemical and particulate (silt) impurity content that gives the layer an amber color (Conway et al., 1996; Holdsworth, 1974). The basal zone can contain other layers of ice facies from 0.5 to 1 meter thick (Fitzsimons, 1999; Holdsworth, 1974). The basal layer exhibits a relatively low viscosity and accommodates up to 60% of the surface velocity of the observed surface displacement (Cuffey et al., 2000; Hubbard et al., *pers comm*. 2005).

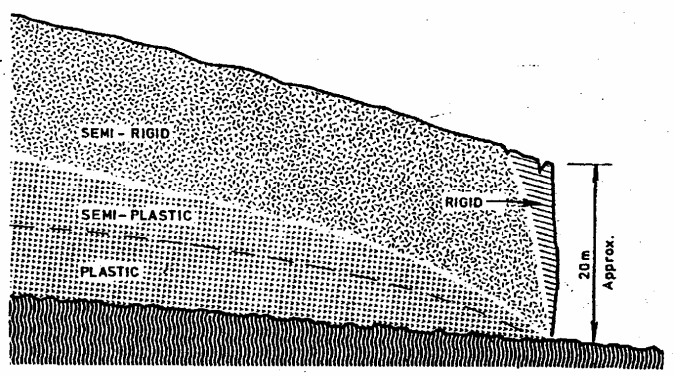

Figure 6: The grounding of the upper semi-rigid, and outer rigid rheological zones result in an impedance to flow and lead to the development of an ice cliff (Chinn, 1985; Holdsworth, 1969). From (Chinn, 1985).

Ice rheology in polar glaciers changes with the thickness of the glacier and affects the terminal morphology of the glacier. As the rigid outer skin of the glacier becomes grounded, it obstructs glacier flow and increases basal shear in a relatively narrow area at the bottom. Since the upper layer of ice is rigid, thinning of the glacier and grounding of the upper layer create a marginal cliff (Chinn, 1991). Once an ice cliff forms, ice debris from calving events and moraine material forms an apron at the base of the cliff. Continued basal shearing and/or glacial advance can continue ramping the active ice up and over the apron in front of the glacier and maintaining a cliffed margin (Figure 7) (Chinn, 1985; Evans, 1989). Studies of an ice cliff in northern Greenland also indicate cliffs are formed due to similar ramping mechanisms at the terminus of the glacier (Goldthwait, 1960, 1961).

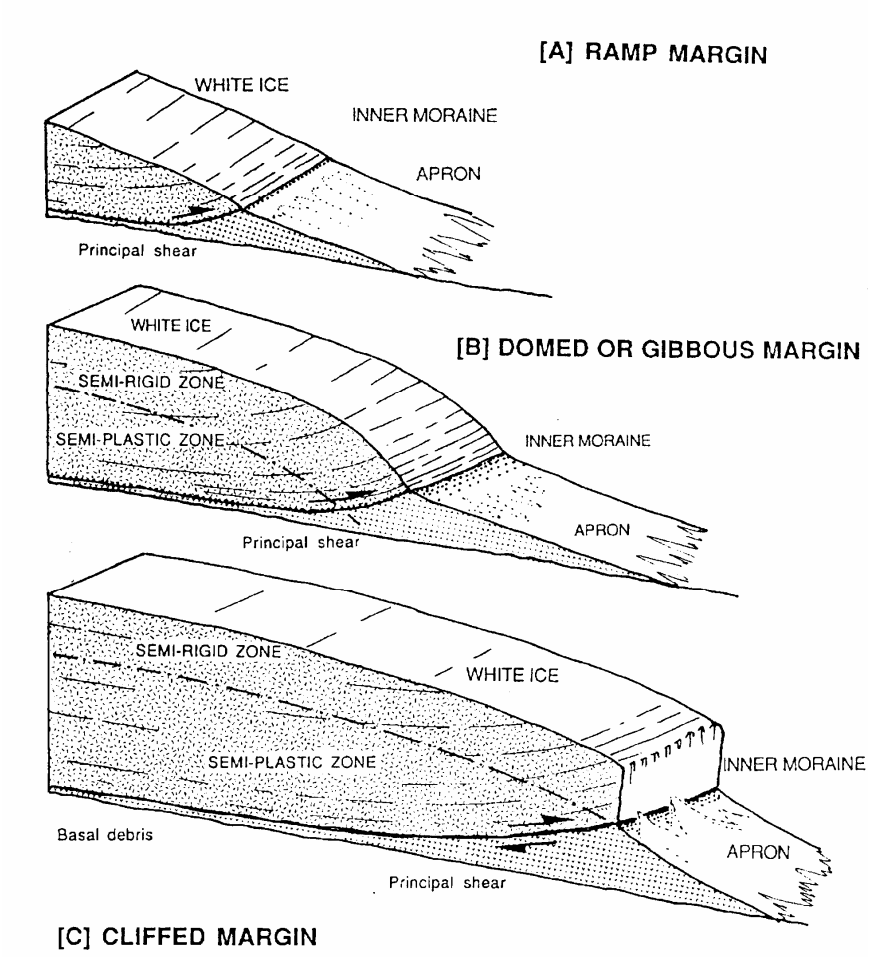

Figure 7: The progression from ramped margin to cliffed margin is a result of the grounding of the upper semi-rigid zone and increased basal shearing and ramping of the glacier ice. From (Chinn, 1991).

A related model suggests that isoclinal folding resulting from marginal basal shear, causes ramped instead of cliffed margins to form (Figure 8). Large-scale isoclinal folds have been observed in polar glaciers of the McMurdo Dry Valleys (Chinn, 1989). Folds forming in the basal shear zone can become overtuned as the glacier overrides the ice apron at the terminus. Continued flow pushes the over-turned fold outward forming a vertical cliff. In this model, vertical cliffs form where folds

are overturned, ramped margins form where folds are absent or in early stages, and domed margins represent stages in between the end members (Chinn, 1985, 1989, 1991). Additional evidence suggests vertical cliffs form in areas when a glacier is locally advancing and ramped margins form where the terminus is retreating (Chinn, 1991).

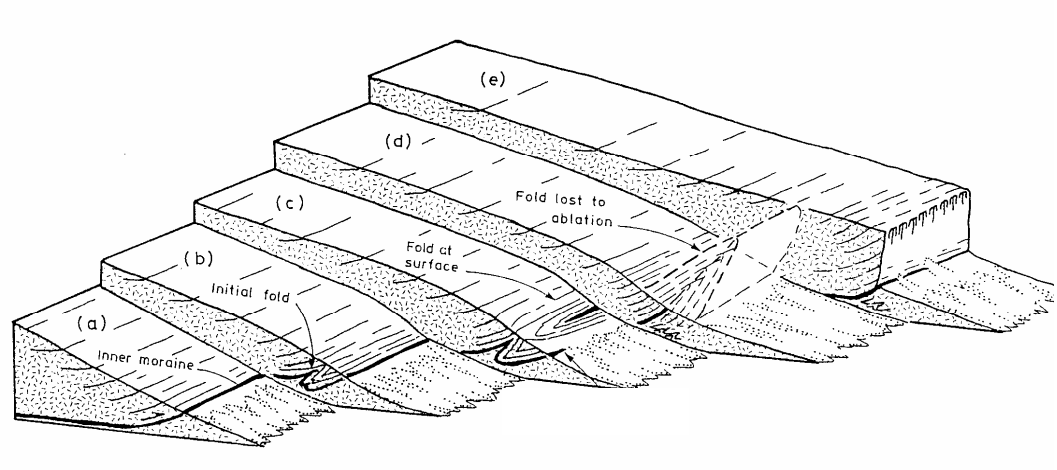

Figure 8: Stages of marginal fold development leading from a ramped terminus (a) to a terminus with a vertical cliff (e). From (Chinn, 1989).

In addition to large-scale structure and ice rheology, a microclimate may have a significant role in the mass balance and morphology of ice cliffs. At high latitudes the sun is low on the horizon. In the McMurdo Dry valleys solar angle is approximately 30° from horizontal in the north and 15° in the south (Johnston, 2004). As a result, solar insolation is more intense on vertical cliffs than on horizontal surfaces nearby. Emitted long wave radiation from the warm valley floor further warms the cliff. Lower wind speeds along the cliff reduces sublimation/evaporation

and increases melt such that ablation can be up to 8 times the value at the surface (Chinn 1987). The increased ablation on the cliff is almost completely due to an increase in melt (Lewis et al., 1999).

Chapter 2: Methods

This project measured ice motion in the lower ablation area and ice cliffs of Taylor Glacier. Stakes were arranged in two different types of arrays, one to measure surface motion and another for motion on the vertical cliffs at the terminus of the glacier. Stake displacements were measured using differential GPS and conventional survey (Total Station) methods. Stakes were placed in 3 locations on the near-horizontal surface of the glacier as well as two locations on the cliff face. Measurements were taken over three summer research seasons in 2003, 2004, and 2005. Ablation measurements were also taken whenever possible. Two other stake arrays were installed on the glacier but are not discussed here. These arrays were installed in 2003 at Site 1a and replaced the following season at Site 1b. Only results from Site 1b are discussed in this analysis.

2.1: Surface Site Networks

Stake networks on the sub-horizontal surface consist of 13 ablation stakes designed to measure strain in three transects. The stakes are made from 2-inch diameter steel conduit (EMT) painted white to reduce heat conduction. The stakes were drilled vertically into the ice to a depth of approximately 2 m using a gasoline-powered drill. At the terminus sites stakes were laid out between five and 25 meters from the cliff edge and arranged as shown in Figure 9.

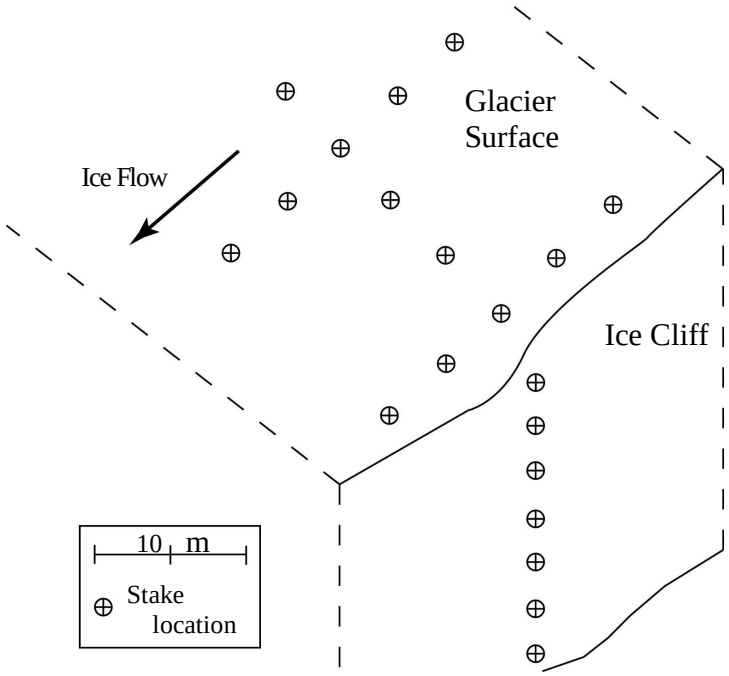

Figure 9: General layout of the two types of arrays used to measure ice flow on the glacier surface and the vertical ice cliff.

The surface networks were measured with dual-frequency Differential GPS (DGPS) with assistance provided by The University NAVSTAR Consortium (UNAVCO) a non-profit organization that provides technical GPS support. The DGPS method measures the distance between two GPS receivers located on the Earth's surface. This method removes several errors associated with GPS using a single receiver including atmospheric and timing errors (Bartel, *pers comm*, 2004). Using DGPS, occupying a stationary location for 8 to 15 minutes can provide a relative location accurate to less than a centimeter.

The surface networks were also measured with a conventional Total Station with assistance provided by Jeffery Scanniello of the Raytheon Polar Services Company (RPSC) Survey Department using A Nikon DTM-502 series Total Station

with a published accuracy of 5 seconds. Control points were established off the glacier north of the cliff. Spikes were driven into the ground to identify each control point and defined a baseline from which to survey the stake network. A reflecting sight glass was placed at the top of each stake to measure distance, and angles were measured to the base of the stake where it entered the glacier surface. To both reduce and quantify instrument error angle, measurements were "doubled" by measuring the angle from the backsight to the foresight with the instrument in "normal" position and a second time with the instrument in the inverse position. Angles were then re-measured using the same method but initiating measurements from the foresight rather than the backsight. The control points were located by differential GPS with a base station located at the established UNVACO benchmark. Stakes from the cliff arrays were measured at different times using a Sokkia Set II total station with an accuracy of 5 seconds.

Three field seasons for this project took place during the Austral summer between 2003 and 2007. Over the duration of the project, 3 stake networks were installed on the surface of Taylor Glacier and 2 arrays were installed in the north-facing cliff at the terminus of the glacier (Figure 10). Stakes within the networks and arrays were measured periodically during the austral summer throughout the duration of the project using differential GPS and a conventional total station. When possible, ablation data was recorded throughout the project for all the stakes.

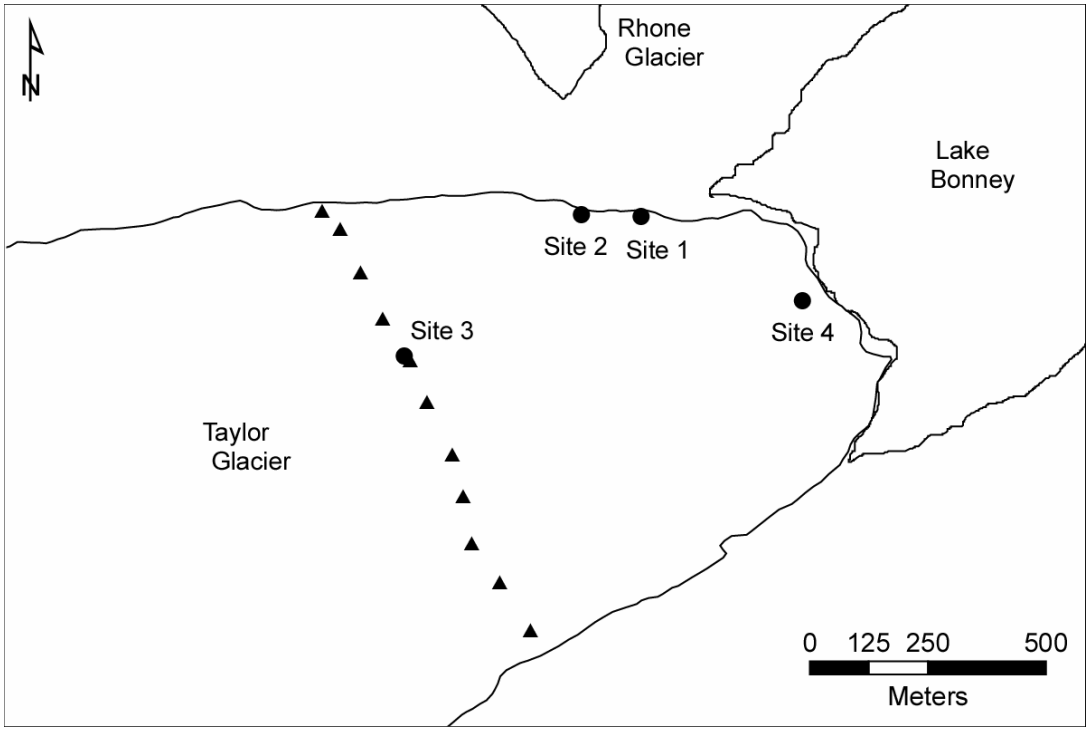

Figure 10: Field site locations on Taylor glacier. Circles represent clusters of 13 stakes and triangles represent individual stakes in a linear transect.

During the second (2004 - 05) field season two surface networks were placed along the northern terminus of Taylor Glacier at Sites 1b and 2. The sites were chosen based largely on cliff morphology. The goal was to find a vertical cliff face 20-30 meters tall, not likely to calve within the time span of the project, and accessible from the surface. No sites on the south side of the glacier were found that matched those criteria. The array at Site 1 was installed to slightly overlap with Site 1a (Figure 11). Due to surface features on the glacier the configuration of stakes in all the surface networks are not identical. Each site has varied slightly from the idealized arrangement of stakes.

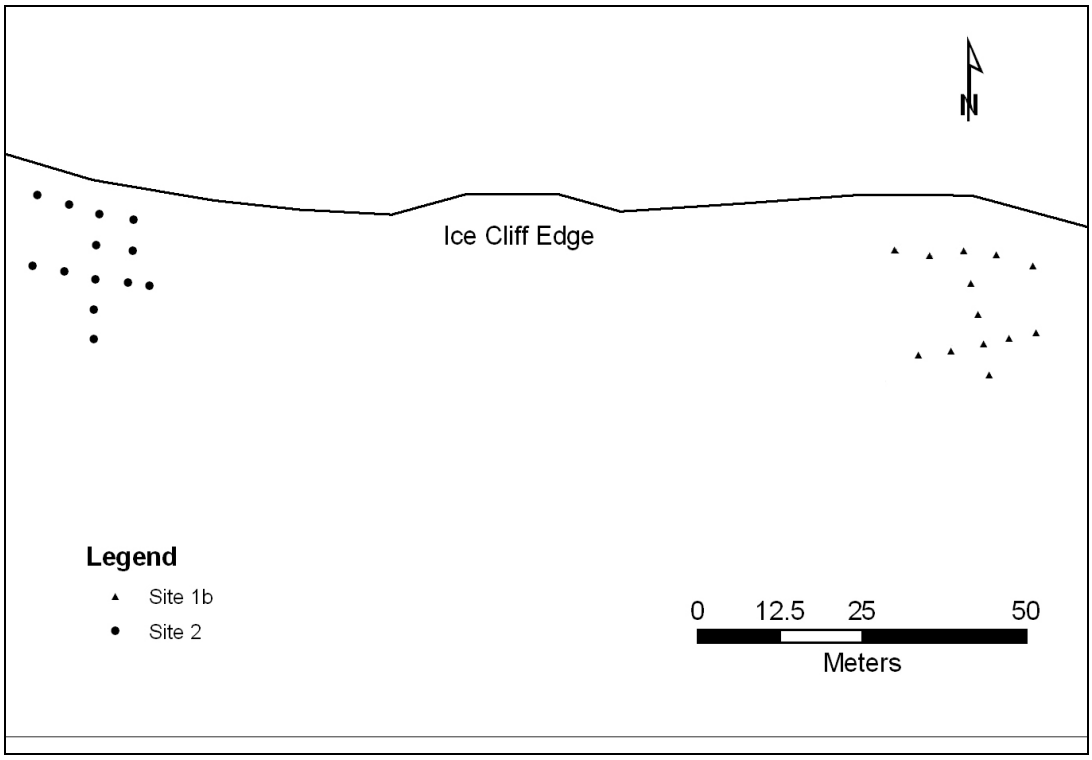

Figure 11: The layout of the cliff sites along the northern cliff of Taylor Glacier. The stake numbering conventions for all sites are the same as in Figure 12 below.

One network was installed in the interior of the glacier. Thirteen stakes in a similar configuration as those at Sites 1 and 2 were installed at Site 3, an interior site well away from the effects of the terminus edge (Figure 12). The surface networks at Sites 1 thru 3 were measured at the beginning and end of the 2004 – 2005 field season with differential GPS.

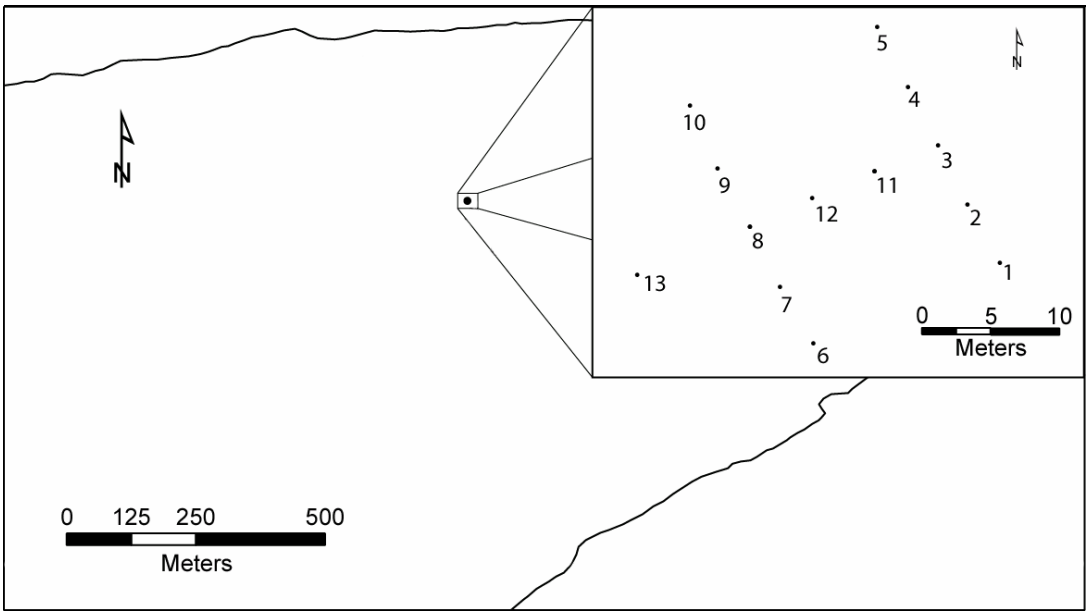

Figure 12: The layout of stakes at Site 3 in the interior of the glacier.

2.2: Vertical Cliff Networks

To measure the development of the vertical cliff profile, two arrays of stakes were installed in the vertical face of the northern terminus of the glacier. The arrays are located on the cliff face below Sites 1 and 2 and consist of 10 stakes vertically aligned in a transect from the top of the cliff to the base with approximately 3 meter spacing (Figure 9). Each stake was drilled into the ice face at about a 10-degree angle to a depth of between 1.75 and 2 m to prevent stakes falling out due to gravity. A survey reflector was permanently attached to the tip of each stake to be used for optical surveys and centimeter hash marks along the stake length allowed measurements of ablation.

Only Total Station measurements were taken for the cliff stakes. The different orientation and perspective, compared to the surface stakes, required a separate baseline for each vertical cliff array. Measurements were taken for each array from

two control points on the ground. The installation of the cliff stakes was difficult. The process involved two field team members rappelling from the cliff simultaneously, two field members at the top of the cliff tending the ropes for the climbers, and two members at the bottom of the cliff managing equipment. Using a gas-powered ice auger they drilled holes in the ice for the stakes. Since the length of the auger bit was so unwieldy while hanging from the ropes, the climbers drilled the holes in four rounds, each using a successively longer bit. Stakes were then inserted into the holes and backfilled with water from a nearby stream to freeze the stakes in place. In all, the process of installing one cliff array (10 stakes) took between 15 and 17 hours.

These vertical arrays were measured using a total station from control points located on the ground. The arrays were measured four times during the second field season on November 28, 2004, December 5, 2004, December 12, 2004, and January 22, 2005.

Chapter 3: Results

3.1: Field Results

One set of stakes was installed at Site 1a and surveyed during the first field season. During the second field season a second set of stakes was installed at Site 1b to overlap with the Stakes at Site 1a. The new stakes were installed to maintain consistency with other new arrays installed during the second field season. As a result, measurements at Site 1a were discontinued. Only data from Site 1b are presented in this analysis and will be referred to as Site 1 hereafter.

The bulk of the fieldwork for the project occurred during the second field season (November 2004 – January 2005). Three stake networks were installed on the surface of the glacier as well as two vertical arrays on the ice-cliff face. Each network and array was measured at least twice during the season, once in the early part of the season and again at the end. Measurements were taken by using two GPS units as rovers within the array and one GPS unit located off the glacier on the ground at an established UNAVCO benchmark recorded by UNAVCO as "NZAP Benchmark TP1 (TP01)," to the northeast of the glacier (Figure 13). This provided a fixed point and served as the primary base station for the remainder of the project for all the sites.

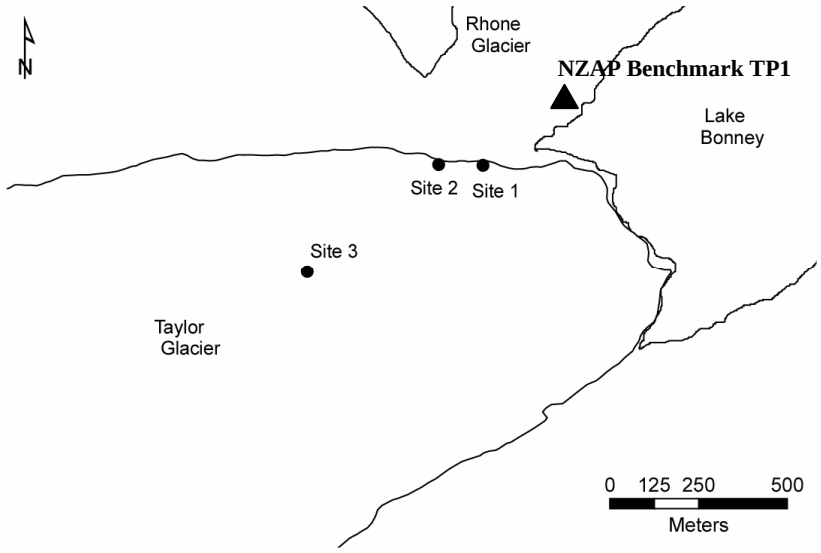

Figure 13: UNAVCO NZAP Benchmark TP1 (triangle) located at 77 43 10.4851 S 162 16 27.985 E in relation to project field site locations.

The surface networks at Site 1 and 2 were measured with optical methods identical to those used in the previous season. All the sites were measured twice during the season. A third control point was established in order to survey the network at Site 2. The network at Site 3 was also measured by optical methods. Site 3 cannot be targeted at a reasonable distance to set control points on the ground, so temporary control points for the optical survey were installed on the glacier surface for each survey.

During season three (November 2005 – January 2006) Matt Hoffman replaced Peter Sniffen on the field team. The largest change over the winter season was a calving event at Cliff Site 1 that destroyed several stakes from the array. Measurements were continued similarly to the first two seasons.

The surface sites were surveyed twice during the third field season using GPS methods. The surveys were done in the same manner as previous field seasons with an off-glacier base station, a local base station on a stake in the network, and a roving GPS unit to measure the remaining stakes. Some arrays lost stakes to calving and ablation throughout the field season.

The calving event at Cliff Site 1 destroyed four stakes from the array and significantly damaged the remaining four. The stakes that remained in the cliff face were bent downwards at an approximately 90-degree angle and were useless. Due to high ablation rates at the cliff face, the stakes were completely melted out by the end of the season.

The stakes at Cliff Site 2 all survived the winter. Stake four at approximately 15 meters up the cliff, sustained a bend between the reflector and the cliff face. Mysteriously neither stake above or below stake 4 showed signs of damage. These stakes were measured as they were in earlier seasons. By January all of these stakes had also melted out of the cliff.

3.2: Surface Velocity

The overall pattern of stake velocities in the lower ablation zone of Taylor Glacier conforms to expectation. Velocities average higher in the interior of the glacier (5.0 ± 0.14 ma^{-1}) and lower along the sides (3.0 ± 0.14 ma^{-1}). The velocity vectors rotate outwards from the centerline for stakes closer to the edge of the glacier (Figure 14). Our results agree with previous measurements on Taylor Glacier (Johnston et al., 2005; Robinson, 1984).

Errors in velocity are reported from a least squares analysis calculated by Trimble Geomatics Office (TGO), the program used to analyze DGPS data. Errors from TGO ranged from 3 mm to 7 mm. A conservative error estimate of 0.01 cm was propagated though the velocity calculations following (Taylor, 1997) to yield an error of ± 0.014 ma^{-1}. This error is applied to all subsequent surface velocities.

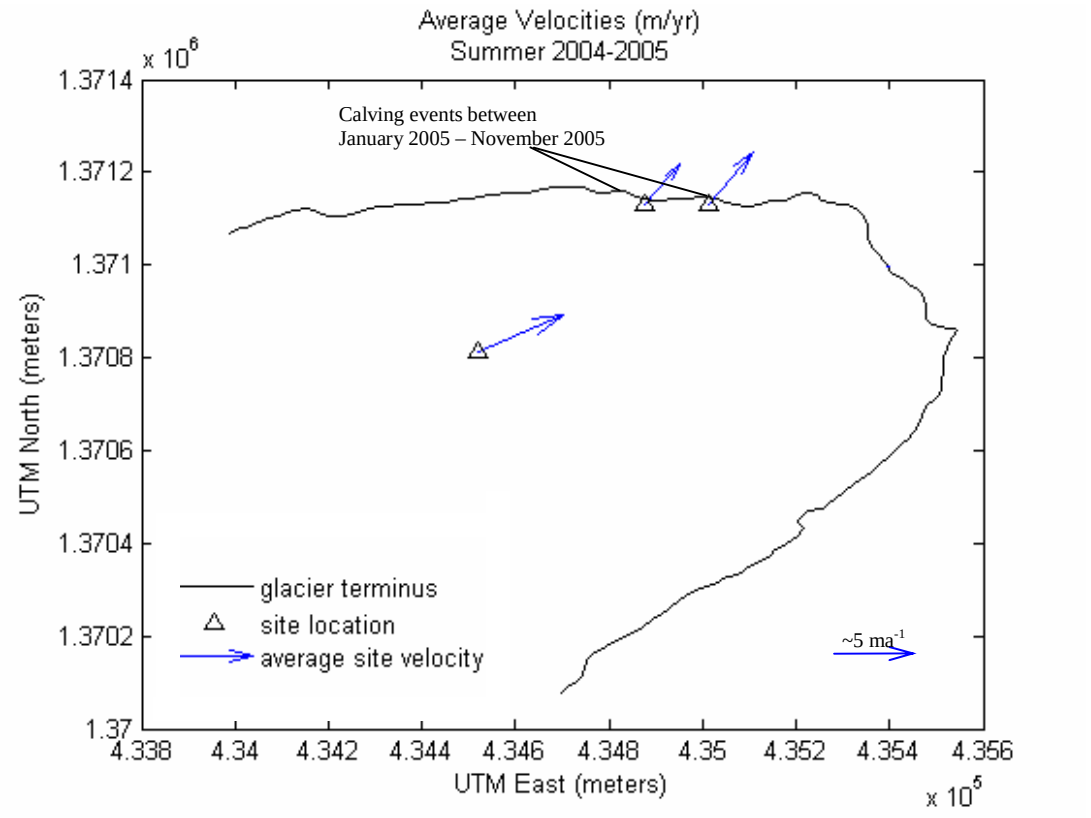

Figure 14: Velocity values during the summer of 2004-2005 for each site in the lower ablation zone of Taylor Glacier. Each triangle and associated velocity represents the average of 13 stakes in that area. Velocity vectors are scaled 40 times and reflect values between 5.0 and 3.0 ma^{-1}.

Velocities at Site 3 show consistent magnitudes and directions throughout the study (Figure 15). There was a slight increase in summer velocity over the study interval increasing from 4.95 ma^{-1} (summer 04-05) to 5.10 ma^{-1} (winter 2005) to 5.28 ma^{-1} (summer 05-06).

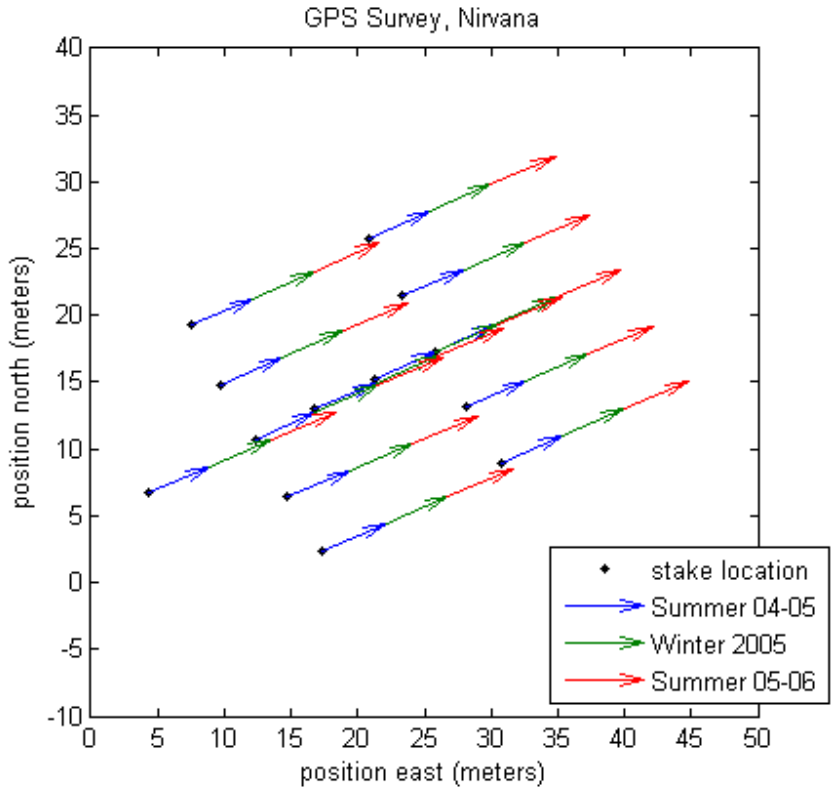

Figure 15: Velocity vectors at Site 3 laid tip to tail for three seasons of study. Note consistent direction and only a slight increase in magnitude throughout the duration of the study.

Velocities at Site 1 and Site 2 are also fairly consistent (summer 04-05 through winter 2005). Velocities at Site 1 average slightly higher, 3.06 ma^{-1}, than those at Site 2, at 2.86 ma^{-1} (Figure 16). The average summer velocity at Site 1 and 2 also increased throughout the study from 3.06 ma^{-1} (summer 04-05) to 3.27 ma^{-1} (summer 05-06) at Site 1 and from 2.86 ma^{-1} to 4.01 ma^{-1} over the same interval. This increase however, is at least partially due to the dramatic increase in velocity of a few stakes at each location.

Stake velocities at Site 1 and Site 2 show an increase in velocity with distance from the cliff edge (Figure 17). This relationship is less well defined in summer than winter (Figure 18). This variability in the summer may have several causes. Stakes

were measured one day after installation during the summer 2004-05 season and some variability may have been introduced if those stakes shifted during refreeze after the first measurement. Also, the measurement interval is two months during the summer and 9 months during the winter. The longer measurement interval over the winter reduces the error associated with the measurement, reducing variability. Finally the variability could be real, suggesting the cliff edge is more active during the warm summer and may behave more erratically during that time.

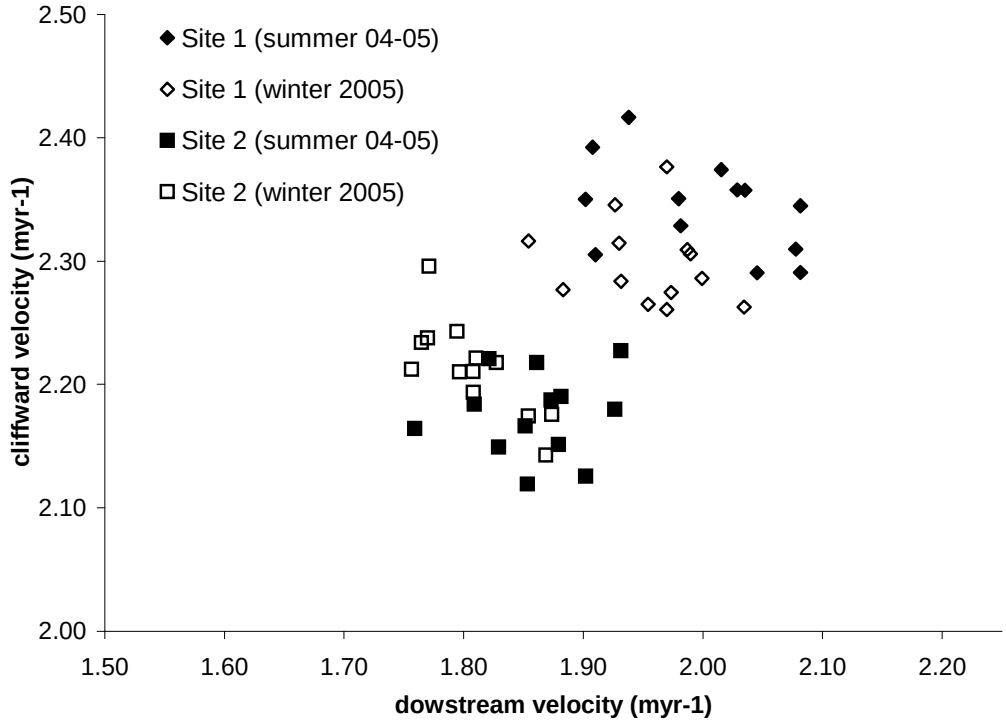

Figure 16: Velocities at Site 1 and Site 2. Site 2 velocities are slightly higher than at Site 1 but there is no significant difference between winter and summer velocities at each site.

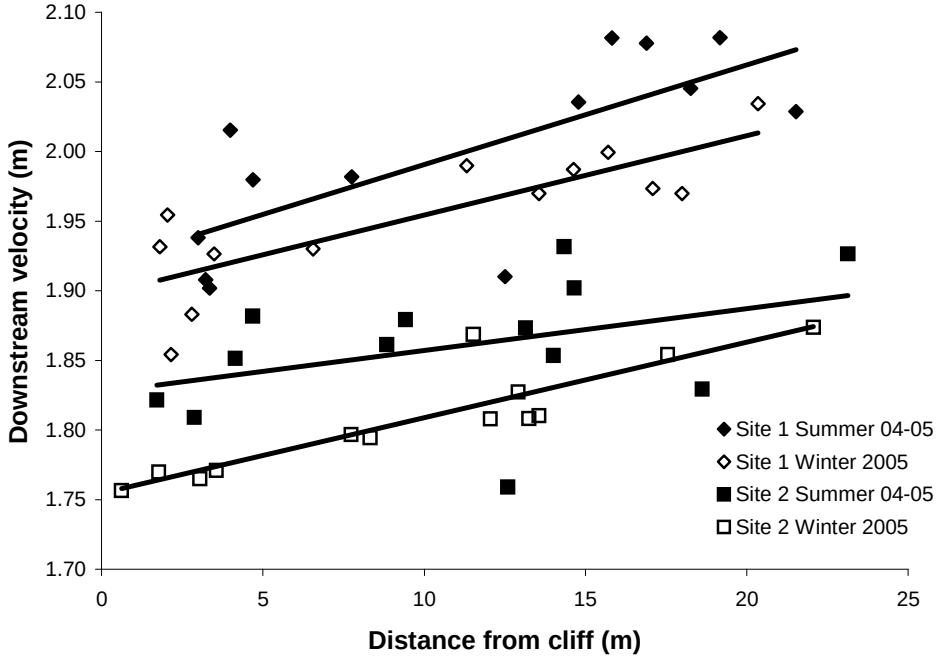

Figure 17: Downstream velocities at Site 1 and 2 show increasing velocity with distance from the cliff for both Summer and Winter seasons.

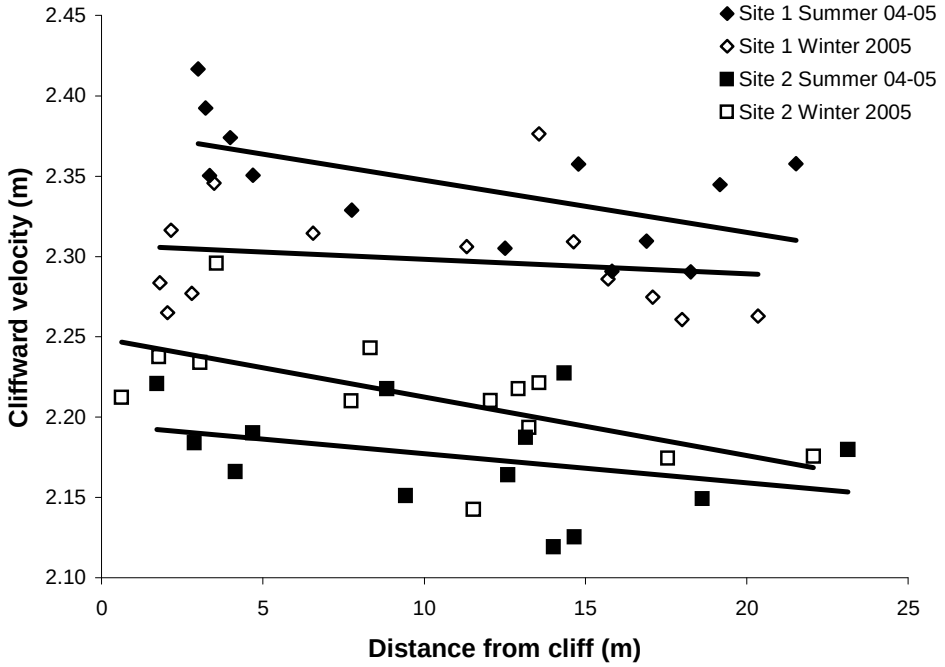

Figure 18: Cliffward velocities at Site 1 and Site 2 show weak trends of decreasing velocity with distance from the cliff for both summer and winter seasons.

Site 1 and Site 2 both show significant changes during the final summer field season (2005-06). Both Site 1 and Site 2 lost several stakes over winter due to melt-out and a major calving event (Site 1). At Site 1 three stakes were lost over the winter season. Excluding stakes 2 and 12, average velocities increased approximately 4% from 3.08 ma^{-1}during summer 2004-2005 to an average of 3.22 $ma^{-1}$the following summer. For stakes 2 and 12 the downstream velocity component decreased from 1.95 $ma^{-1}$and 1.99 ma^{-1} (summer 04-05) to 0.78 $ma^{-1}$and 0.74 ma^{-1} (summer 05-06), respectively. The cliff-ward velocity component increased from 2.39 $ma^{-1}$and 2.31 $ma^{-1}$to 3.46 $ma^{-1}$and 3.37 ma^{-1}over the same time period (Figure 19). It is interesting to note that stakes 2 and 12 are not adjacent to each other and that immediately neighboring stakes (stakes 3 and 11) did not experience the same change in motion.

Site 2 experienced changes similar to Site 1. Three stakes in positions close to the cliff were also lost at Site 2 (stakes 3, 4, and 5). Site 2 experienced a 6% increase in velocity from 2.86 ma^{-1} (summer 04-05) to an average of 3.05 $ma^{-1}$the following summer. The velocities of three stakes also changed dramatically similar to those at Site 1. Downstream velocity at stakes 2, 6, and 11 decreased to 0.70 ma^{-1}, 0.93 ma^{-1}, and –0.02 ma^{-1}. Cliff-ward velocity for these stakes increased accordingly to 5.86 ma^{-1}, 3.76 ma^{-1}, and 8.95 ma^{-1}, respectively (Figure 20). Similar to Site 1, the stakes that changed motion dramatically do not expose a pattern associated with spatial distribution or proximity to the cliff. Stake 6 in this case was located at least 15 meters from the cliff edge yet experienced a similar increase in cliff-ward velocity to stakes only 5 meters from the edge.

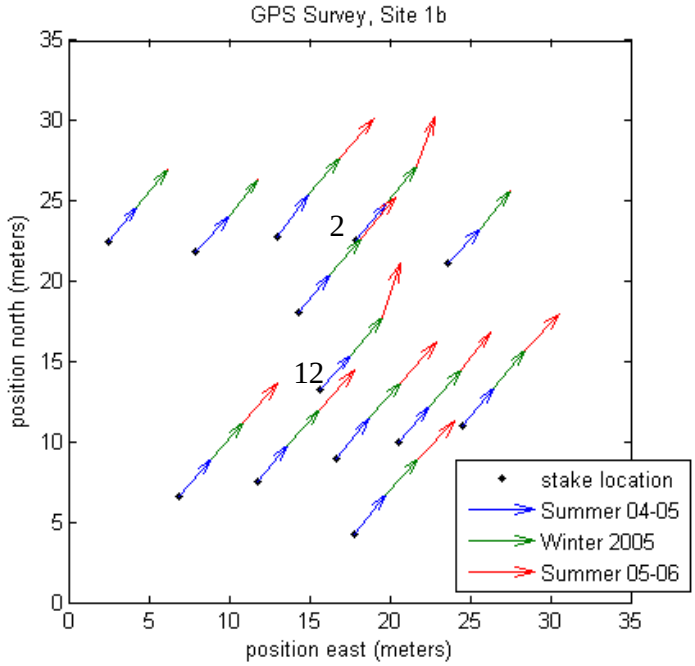

Figure 19: Velocity vectors for three seasons at Site 1 plotted head to tail in chronological order. There is little change during the first two seasons (blue and green arrows), however the motion of stakes 2 and 12 (labeled) changes dramatically during the second summer (red arrows).

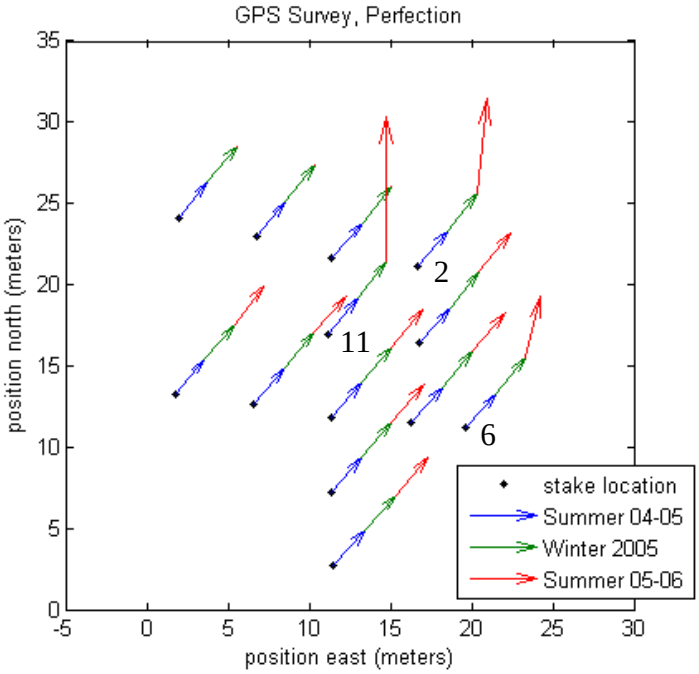

Figure 20: Velocity vectors for three seasons at Site 2 (Perfection) plotted head to tail in chronological order. Note the dramatic change in velocity for stakes 2, 6, and 11 (labeled) that occurred during the summer season of 2005-06 (red arrows).

Chapter 4: Analysis

Two separate dynamics are active at Site 1 and Site 2. The underlying pattern is associated with an increase in downstream velocity with distance from the cliff edge. The pattern of increasing downstream velocity with distance from the cliff is, however, consistent with simple shear (Figure 21).

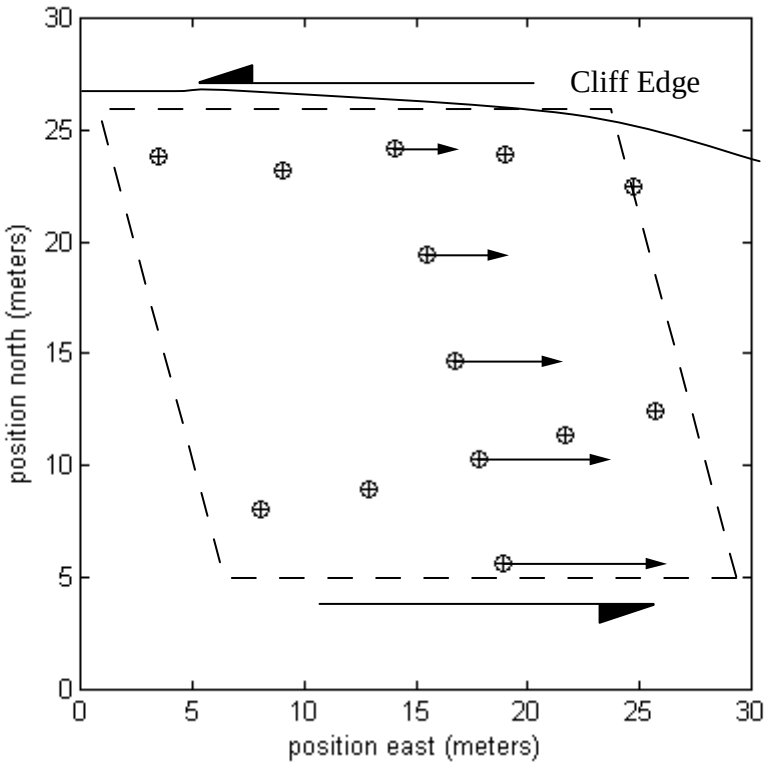

Figure 21: A pattern of increasing downstream velocity with distance from the cliff edge indicates a stress regime consistent with simple shear. Dotted line represents a square deformed through left-lateral shear consistent with observed stake motion.

The second emergent pattern was observed in the summer 2005-06 season. During this time, velocities at Site 1 and Site 2 increased. In addition, the velocities of several stakes drastically increased in their cliff-ward component while simultaneously decreasing in the downstream component. This suggests a decoupling between the

main body of the glacier and the ice immediately surrounding these stakes. At Site 1 there was a calving event during the previous winter and at Site 2 a calving event also occurred nearby. The change in velocities may be reactions of the ice to these local events.

It is also plausible that as the stakes flow closer (within meters) to the cliff edge the ice is increasingly under the influence of the local stress regime at the edge of the cliff. This does not explain why the pattern of velocity change is not consistent, however. At Site 1 the dramatic change in velocity was shown for stake 2 but not for stake 3, which is located only 5 meters away and at the same distance from the cliff. At Site 2 stakes 2 and 11 are located close to the cliff edge and show an increase in cliff-ward velocity but stake 6 that is located at least 15 meters from the cliff edge also shows this increase. The behavior of stake 6 could be explained by an observed topographic depression that may influence ice-flow locally.

The dynamics at the cliff edge are complicated and may react strongly to local topography and terminus morphology. Local deformation may occur along existing fractures leading to irregular deformation, explaining dramatic changes at one stake location but not at a nearest neighbor. Deformation and major velocity changes are most likely to occur near to the cliff edge but is clearly not exclusive to change as far as 15 meters from the edge. Local conditions, rather than larger ice-flow dynamics may be the major driving factor to deformation in areas near the cliff.

4.1: Strain Rate

Calving necessarily occurs in an extensional stress regime. In a normally compressional regime at the terminus of a glacier there must be a zone where the deviatoric stress changes from positive to negative. A two-dimensional model for polar ice cliffs predicts this transition occurs between 5 and 20 meters from the cliff edge (Pettit, *pers comm.*). In order to locate this transition zone, I calculate strain rate and principle stain axes for four zones within the stake arrays at Sites 1, 2, and 3. Principle strain axes define two perpendicular lines within a deformed body that represent the maximum and minimum extension or compression in the body.

Two-dimensional strain rate was calculated from velocities measured at Site 1, Site 2, and Site 3. The numerical method follows Malvern, 1969. Strain rate is represented by a two-dimensional square matrix:

$$E = \begin{vmatrix} \dot{\varepsilon}_{xx} & \dot{\varepsilon}_{xy} \\ \dot{\varepsilon}_{yx} & \dot{\varepsilon}_{yy} \end{vmatrix} \qquad \textbf{(1)}$$

where:

$$\dot{\varepsilon}_{xx} = \frac{du}{dx}, \qquad \dot{\varepsilon}_{yy} = \frac{dv}{dy}, \qquad \dot{\varepsilon}_{xy} = \dot{\varepsilon}_{yx} = \frac{1}{2}\left[\frac{dv}{dx} + \frac{du}{dy}\right] \qquad \textbf{(2)}$$

where u is the velocity in the x-direction and v is the velocity in the y-direction

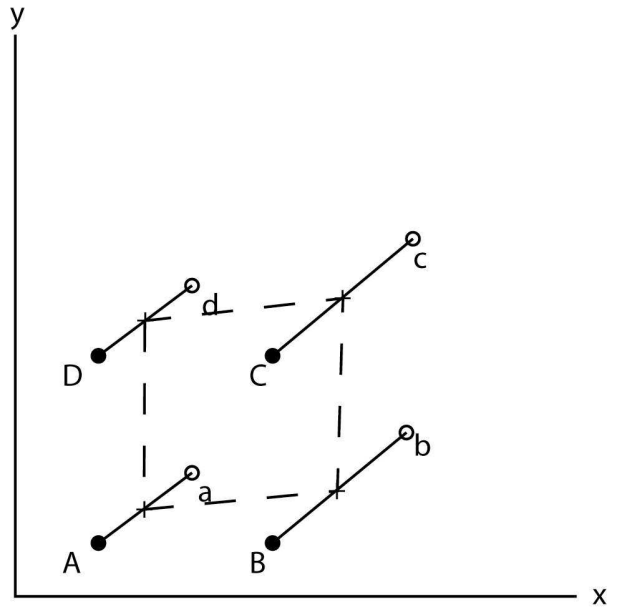

Figure 22: Diagram showing generalized strain quadrangle. Capital letters and solid circles represent the original position of stakes while lower case open circles are final positions. The dotted square represents the area for which strain is calculated. Because we use average velocities, the strain is calculated at the average stake position.

This method is based on *velocity gradients*. Letter subscripts in the following equations refer to the stake positions in Figure 22.

$$\frac{du}{dx} = \frac{1}{2}\left[\left(\frac{u_c - u_d}{x_c - x_d}\right) + \left(\frac{u_b - u_a}{x_b - x_a}\right)\right]$$
$$\frac{dv}{dx} = \frac{1}{2}\left[\left(\frac{v_c - v_d}{x_c - x_d}\right) + \left(\frac{v_b - v_a}{x_b - x_a}\right)\right] \qquad \textbf{(3)}$$
$$\frac{du}{dy} = \frac{1}{2}\left[\left(\frac{u_a - u_d}{y_a - y_d}\right) + \left(\frac{u_b - u_c}{y_b - y_c}\right)\right]$$
$$\frac{dv}{dy} = \frac{1}{2}\left[\left(\frac{v_a - v_d}{y_a - y_d}\right) + \left(\frac{v_b - v_c}{y_b - y_c}\right)\right]$$

These results are then used with equations 1 and 2 to create the two-dimensional strain tensor:

$$E = \begin{vmatrix} \frac{du}{dx} & \frac{1}{2}\left[\frac{dv}{dx} + \frac{du}{dy}\right] \\ \frac{1}{2}\left[\frac{dv}{dx} + \frac{du}{dy}\right] & \frac{dv}{dy} \end{vmatrix} \quad \textbf{(4)}$$

Calculating the eigenvalues and eigenvectors of each strain tensor gives the magnitude and direction of the principal strain axes.

The stake layout of the surface arrays on Taylor Glacier limits strain calculations to four non-overlapping quadrangles in each stake array (Figure 23). Complete data is available from three measurement periods representing the beginning of summer 2004-2005, end of summer 2004-2005, and beginning of summer 2005-2006 for sites 1 and 2. From that data I calculate strain rates for one summer season and one winter season. Site 3 has one additional complete data set, which allows for calculations representing summer 2005-2006 at that site.

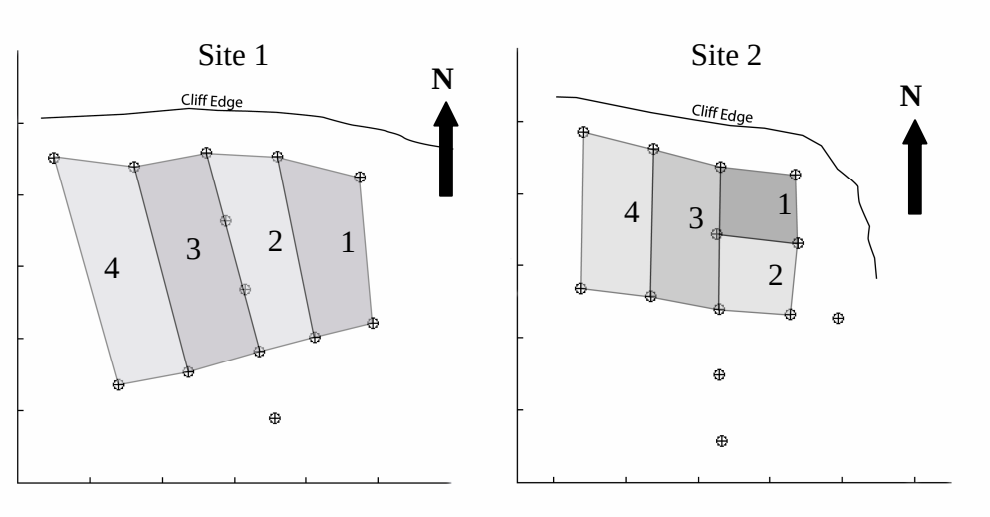

Figure 23: Schematic of non-overlapping quadrangles used for strain rate calculations at Site 1 and Site 3 (left) and Site 2 (right). The quadrangles are numbered for future reference. Site 3 was arranged identically to site 1b.

Summer strain rates at Site 1 range from -0.002 a^{-1} to 0.003 a^{-1} (Table 1). Errors for the strain rate calculations are on the order of 10^{-3} a^{-1} and are discussed at the end of this section. Primary strain axes are extensional and oblique to the cliff. Winter strain rates are slightly lower, ranging from –0.003 a^{-1} to 0.002 a^{-1}. Primary strain axes during the winter are oblique to the cliff but not consistently extensional. Quadrangles 1 and 2 show compression in the primary strain axis (Figure 24).

Table 1: Table of strain rate values and strain axes calculated for two seasons at Site 1. Winter values are shaded in the table. Quadrangle number refers to Figure 22.

	Quadrangle Number	Primary Strain Rate a^{-1}	Primary Strain Axes		Secondary Strain Rate a^{-1}	Secondary Strain Axes	
			X	Y		X	Y
Summer 2004-2005	1	0.001	-0.47	0.88	-0.000	-0.88	-0.47
	2	0.004	-0.49	0.87	-0.002	-0.87	-0.49
	3	0.002	0.00	1.00	-0.001	-1.00	0.00
	4	0.003	-0.81	0.58	-0.000	-0.58	-0.81
Winter 2005	1	-0.003	-0.74	0.67	0.001	-0.67	-0.74
	2	-0.001	0.39	0.92	0.000	-0.92	0.39
	3	0.002	-0.97	0.24	-0.000	-0.24	-0.97
	4	0.002	-0.75	0.66	-0.001	-0.66	-0.75
* error for strain rates is estimated at a magnitude of 10^{-3}							

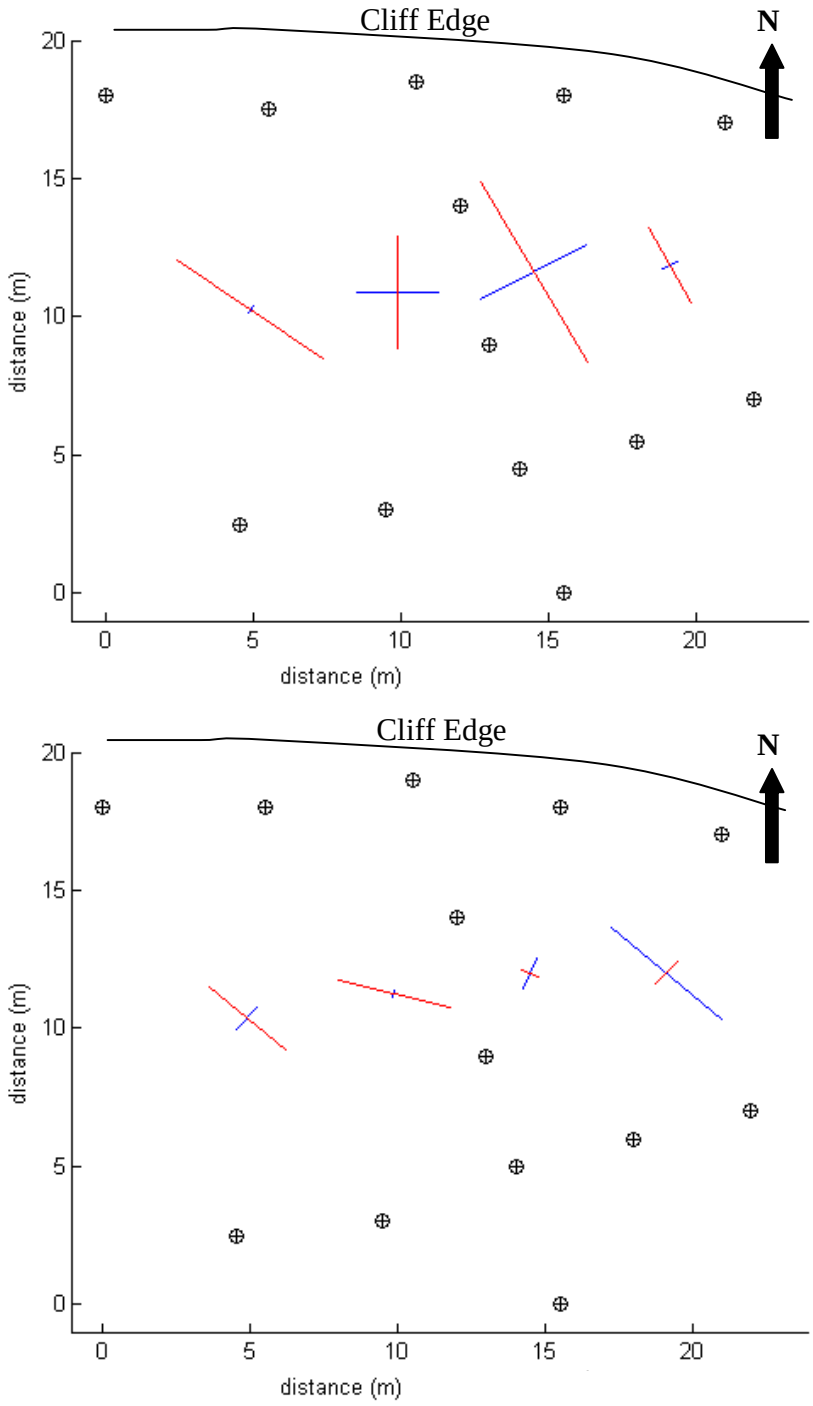

Figure 24: Principle strain rates calculated at Site 1 for summer of 2004-2005 (upper graph) and winter 2005 (lower graph) seasons. Red lines indicate extensional strain while blue represents compressional strain. The strain ellipses are scaled by x10^{-3} a^{-1}.

Strain rates at Site 2 during the summer of 2004-2005 range from –0.001 a^{-1} to 0.004 a^{-1}. As at Site 1, the strain axes are oblique to the cliff edge and extensional. Winter strain rates are slightly lower again, ranging from -.003 a^{-1} to 0.002 a^{-1}. Similar to Site 1, two of the quadrangles (1 and 2) show compression in the primary strain axis during the winter (Table 2), (Figure 25).

Table 2: Table of strain rate values and strain axes calculated for two seasons at Site 2. Quadrangle number refers to Figure 22.

	Quadrangle Number	Primary Strain Rate a^{-1}	Primary Strain Axes		Secondary Strain Rate a^{-1}	Secondary Strain Axes	
			X	Y		X	Y
Summer 2004-2005	1	0.001	-0.95	0.31	-0.001	-0.31	-0.95
	2	0.002	-1.00	-0.03	0.000	0.03	-1.00
	3	0.002	-0.71	0.70	-0.001	-0.70	-0.71
	4	0.003	-0.99	0.10	0.001	-0.10	-0.99
Winter 2005	1	0.002	0.18	0.98	0.000	-0.98	0.18
	2	0.001	-0.27	0.96	-0.001	-0.96	-0.27
	3	0.001	-0.66	0.75	0.000	-0.75	-0.66
	4	0.001	-0.14	-0.99	-0.001	-0.99	0.14
* error for strain rates is estimated at a magnitude of 10^{-3}							

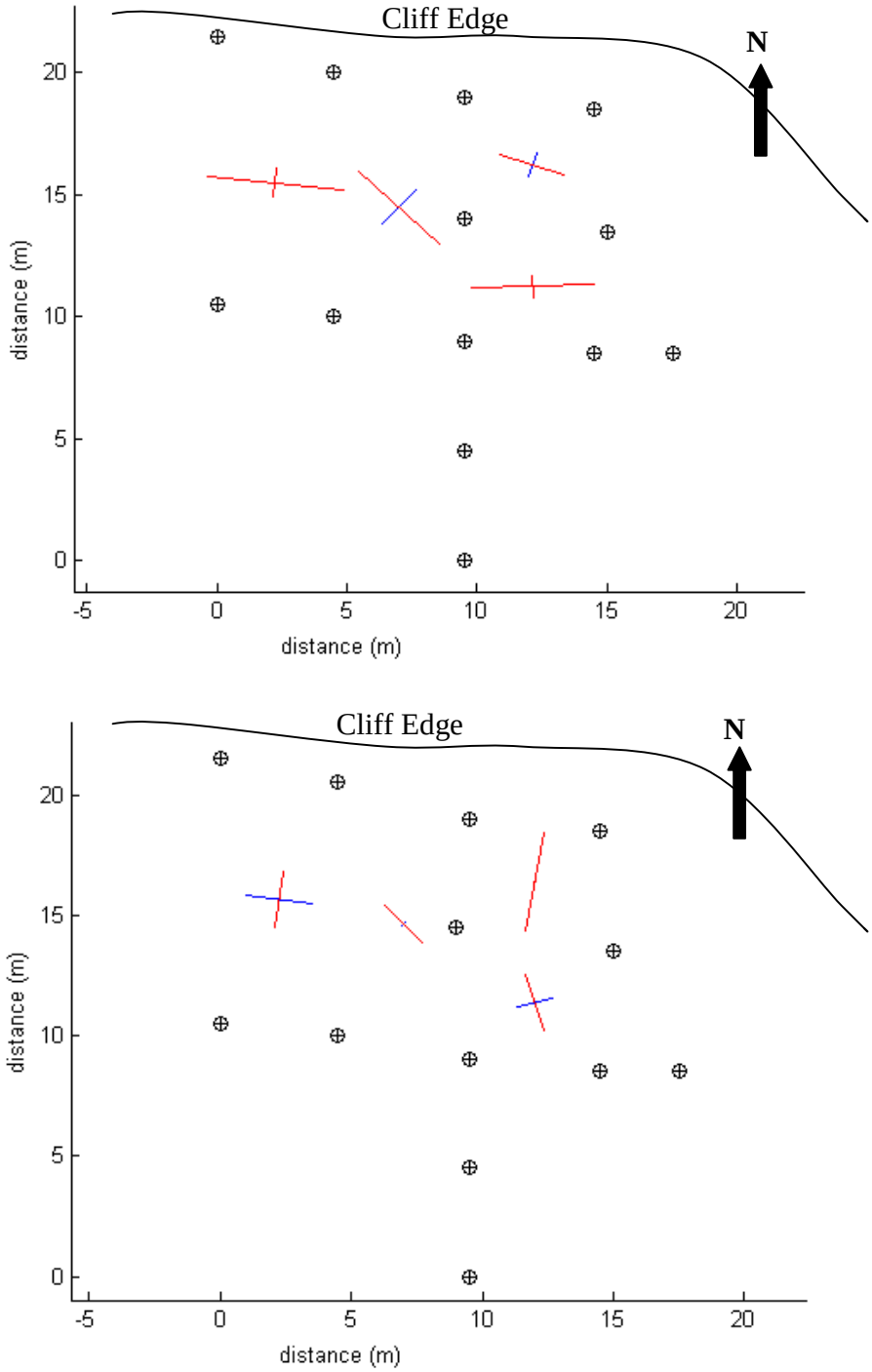

Figure 25: Principle strain rates calculated at Site 2 for the summer of 2004-2005 (upper graph) and winter 2005 (lower graph) seasons. Red lines indicate extensional strain while blue represents compressional strain. The strain ellipses are scaled by $1x10^{3}$ a^{-1}.

Site 3 has a longer data set which allows calculation of strain rates over three seasons: summer 2004-2005, winter 2005, and summer 2005-2006. The strain rates for the first summer season are surprisingly high, ranging from –0.007 a^{-1} to 0.012 a^{-1} (Figure 26). This is most likely due to the stakes shifting positions as they refroze after installation. Stakes at Site 3 were drilled and installed hours before the first survey and probably had not established permanent connection to the glacier leading to later settling and anomalous motion.

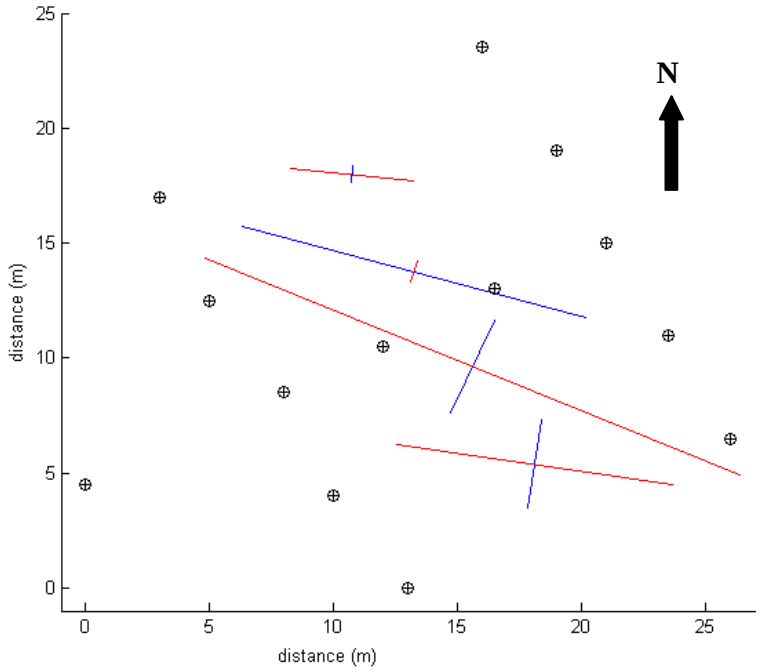

Figure 26: Principle strain rates calculated at Site 3 for the summer of 2004-2005. The anomalously high strain rates during this measurement period are attributed to the shifting of stakes as they refroze after initial measurement. The strain ellipses are scaled by $1x10^3$ a^{-1}.

The winter 2005 strain rates are closer to expectations with values from –0.001 a^{-1} to 0.002 a^{-1}. The strain rates measured during the summer of 2005-2006 are slightly higher than the winter values, and range from –0.003 a^{-1} to 0.003 a^{-1} (Table 3), (Figure 27).

Table 3: Table of strain rate values and strain axes calculated for three seasons at Site 3. Winter values are shaded in the table. Quadrangle number refers to Figure 22.

	Quadrangle Number	Primary Strain Rate	Primary Strain Axes		Secondary Strain Rate	Secondary Strain Axes	
			X	Y		X	Y
Summer 2004-2005	1	0.006	-0.99	0.15	-0.002	-0.15	-0.99
	2	0.012	-0.92	0.40	-0.002	-0.40	-0.92
	3	-0.007	-0.96	0.28	0.000	-0.28	-0.96
	4	0.002	-0.99	0.11	0.000	-0.11	-0.99
Winter 2005	1	-0.001	-0.92	-0.40	0.000	0.40	-0.92
	2	0.000	-0.53	0.85	0.000	-0.85	-0.53
	3	0.001	-0.95	0.32	-0.001	-0.32	-0.95
	4	0.002	-1.00	0.00	0.000	0.00	-1.00
Summer 2005-2006	1	0.001	-0.81	-0.59	-0.001	-0.59	0.81
	2	0.003	-0.81	0.58	-0.003	-0.58	-0.81
	3	0.002	-1.00	0.06	-0.001	-0.06	-1.00
	4	0.002	-0.85	-0.53	-0.002	0.53	-0.85

* error for strain rates is estimated at a magnitude of 10^{-3}

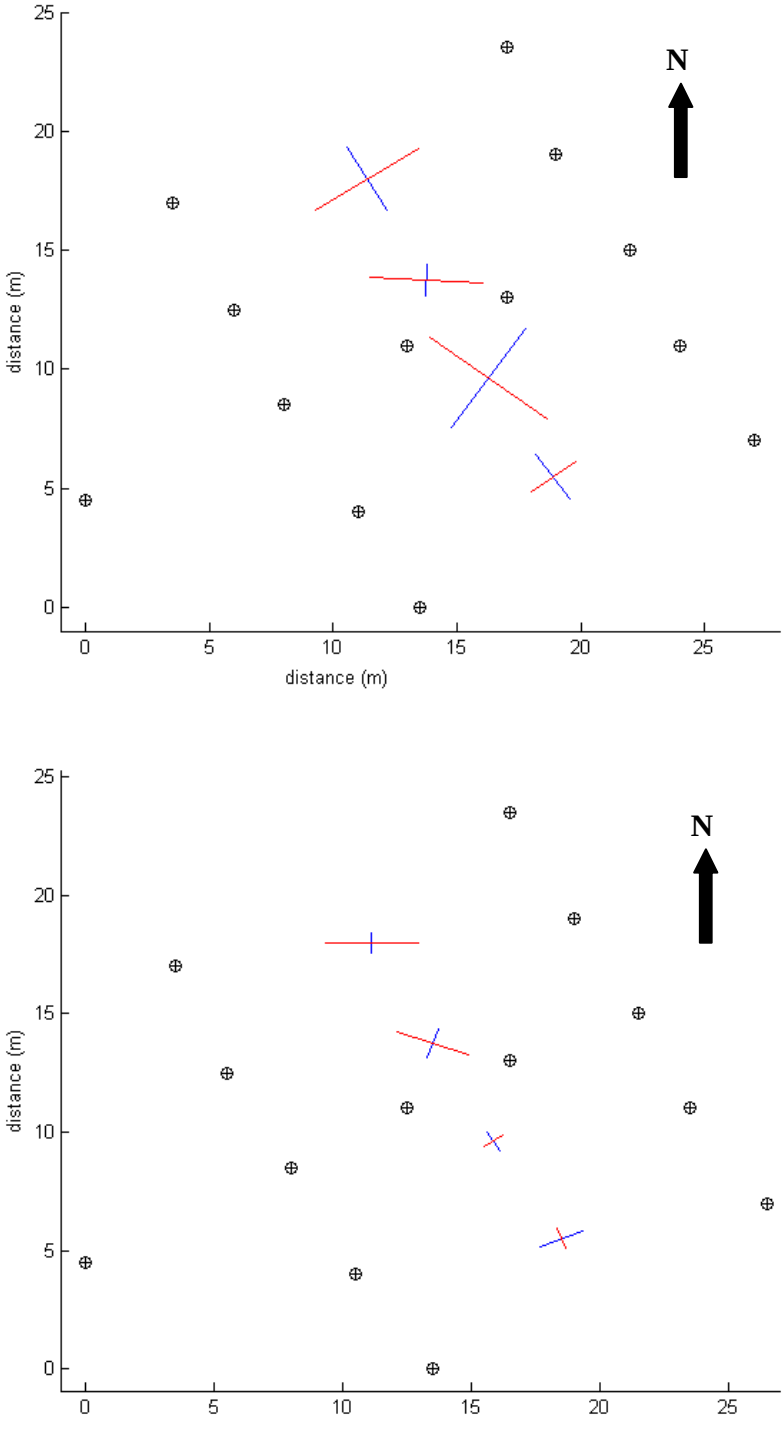

Figure 27: Principle strain rates calculated at Site 3 for the summer of 2005-2006 (upper graph) and winter 2005 (lower graph) seasons. Red lines indicate extensional strain while blue represents compressional strain. The strain ellipses are scaled by $1x10^3$ a^{-1}.

The strain rates calculated for all the sites on Taylor Glacier are inconclusive. The strain rates for all sites fall with the range of $-0.003\ a^{-1}$ and $0.004\ a^{-1}$. But conservative estimates of error for the strain calculation is $0.016\ a^{-1}$. Even a generous estimate of error yields a value of $0.004\ a^{-1}$. At best, the error for the strain calculation is the same order of magnitude as the calculated values and the majority of calculated values fall below the error estimation. Thus I cannot say confidently that the values are different from zero. However, the plotted strain rates are not completely random, suggesting there may be a trend in the calculated values.

Having recognized the problem with measurement error, strain rates at all three surface sites show two general patterns. The first pattern that emerges is that summer strain rates are slightly larger than winter strain rates. The second pattern is during the summer at both cliff sites the primary strain rate axes are extensional and oriented at an oblique angle to the cliff. During the winter the patterns become less clear and half of the primary strain rates become extensional.

Site 3 was included in this study to serve as a baseline to reference the ice behavior at the cliff sites. Site 3 should be free from any effects the vertical cliffs may have on ice flow. Discounting strain rates from the first summer season as anomalous, Site 3 shows slightly lower strain rate values than the other two sites. Similar to the two cliff sites, it also shows there is lower strain rate during the winter season than summer. Strain rates at Site 3 are slightly lower on average than at the other sites. The difference is less than expected and may not be enough to statistically

differentiate between the three surface sites. This could be taken as evidence that the cliffs do not have a large effect on the local stress regime in the ice.

Finally, it is worth mentioning that there is evidence of ice fracture at each of the cliff sites. Fractures measured during the summer of 2004-2005 at the sites had apertures between two and ten centimeters and were oriented at 30-40 degrees to the cliff edge. The fracture patterns are generally consistent with the patterns of the summer principle strain rates at both cliff sites. This indicates the calculated strain values may be significant despite the problematic error estimation.

4.2: Fracture Surveys

During the 2004-2005 season we noticed there were a large number of small fractures in the ice at each of the sites. We decided to make simple fracture maps with the goal of recording where the largest fractures were in relation to the ablation stakes we installed to measure ice motion. The methods of recording the fracture data consisted of hand sketching the sites as well as measuring the aperture and the trend of each fracture. To do this I laid a tape measure on the ice between two stakes in the network and measured each fracture with an aperture of greater than 2-3 mm that intersected the tape. I collected data that includes distance of the fracture along the transect defined by the measuring tape, trend (measured with a Brunton compass), and aperture. One survey was performed at Sites 1through 4 each field season.

There was a significant change between field seasons in the fracture patterns at both Sites 1 and 2. At Site 1 the fractures were largely oriented at a 30-40 degree angle to the cliff edge (Figure 28). The fracture pattern was not clear at Site 2,

however the fractures at this Site were also oriented at oblique angles to the cliff edge consistent with a shear margin (Figure 30). Over the austral winter season of 2005, fracture patterns at both sites changed orientation, becoming more cliff-parallel (Figure 29 and Figure 31). Although nearly all the recorded fractures at Site 1 experienced this change, the fractures within 15 meters of the cliff edge changed most dramatically, becoming nearly cliff parallel. The change was less dramatic at Site 2, however the change was similar and was again mostly expressed within 10-15 meters of the cliff edge.

Ice flow and calving events may have both affected the strain field and therefore the fracture patterns at both Sites 1 and 2. In both locations the stake array moved closer to the cliff edge as the glacier flowed under normal conditions. Velocities near the margins of Taylor Glacier in this region are approximately 2-3 ma^{-1}, bringing the entire stake array closer to the edge by several meters. This put the arrays in slightly different stress fields closer to the cliff, which may have affected the fracture patterns.

There were two calving events along the northern glacier margin in proximity of both sites. One occurred along the cliff edge directly at Site 1 and caused the loss of several stakes in the vertical cliff array and may have caused the loss of stakes 3 and 4 in the surface array. The second calving event was 50-100 meters east of Site 2. In both cases the change in fracture pattern could have been caused prior to the events as stress conditions changed leading up to the events, or alternatively the fractures may have changed orientation as the ice shifted in response to the calving events.

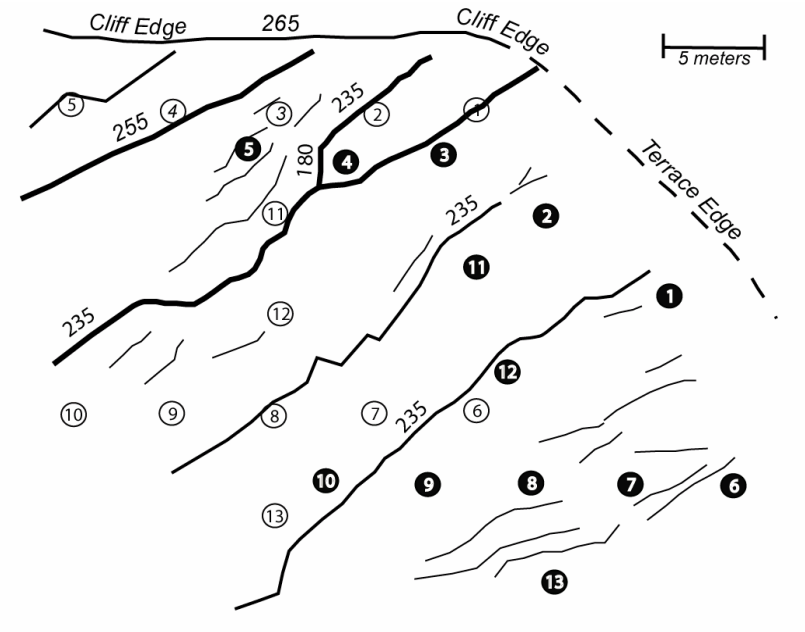

Figure 28: Surface Site 1 2004-2005 season. Based on field sketch and measurements taken by Peter Sniffen.

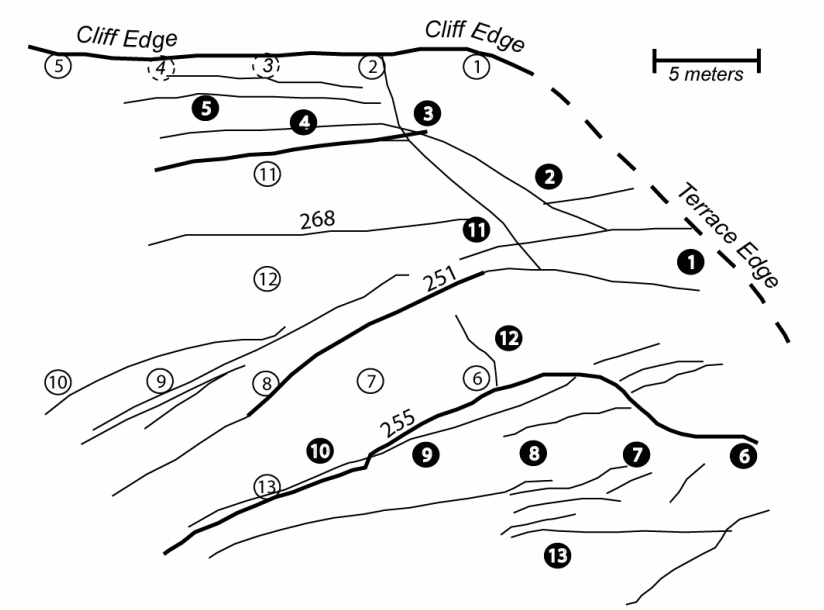

Figure 29: Surface Site 1 2005-2006 season. Dashed circles represent stakes lost to melt-out or calving. Based from field sketch and measurements taken by Matt Hoffman

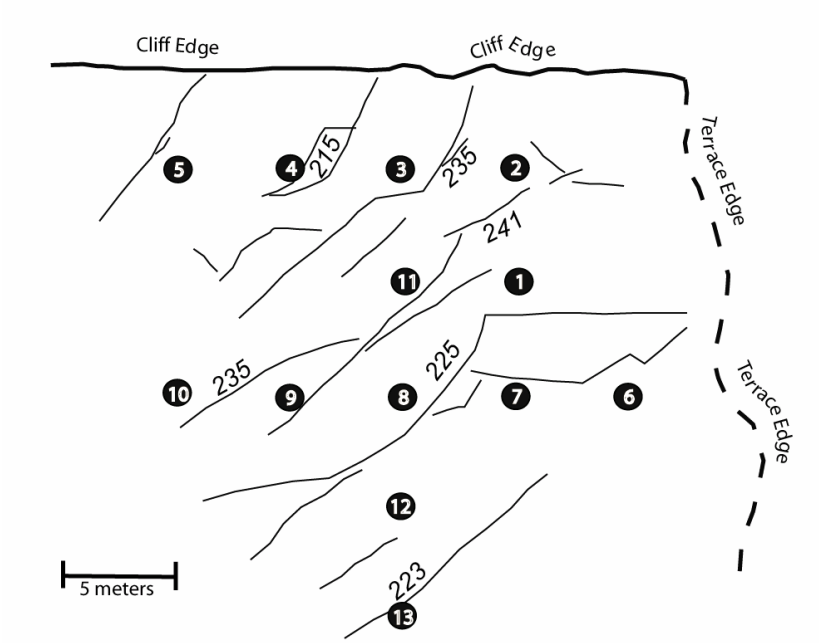

Figure 30: Fracture map of Surface Site 2, 2004-2005 season. From field sketch and measurements by Peter Sniffen.

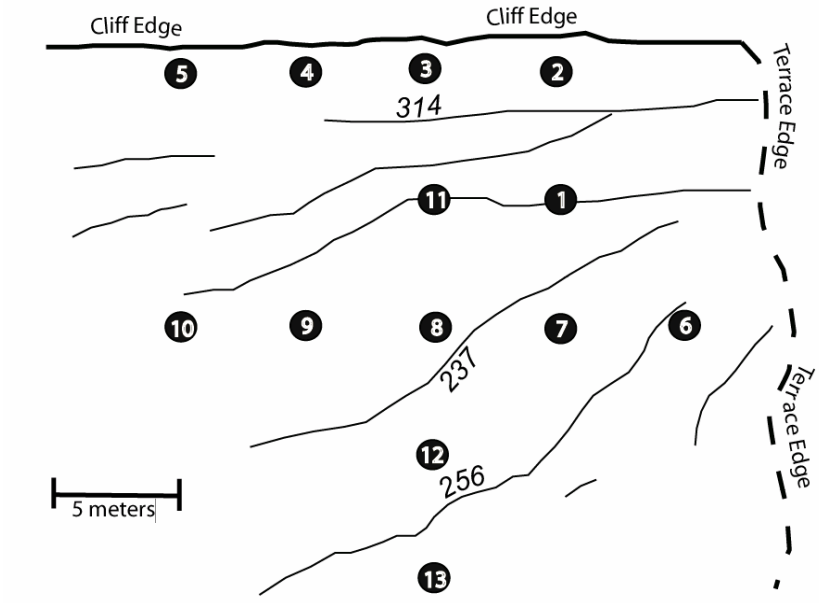

Figure 31: Fracture map of surface Site 2 from the 2005-2006 season. From field sketch and measurements collected by Matt Hoffman.

4.3: Vertical Cliff Sites

Ablation and ice flow data are available for the summer of 2004-2005 and winter of 2006 for both Cliff Site 1 and Cliff Site 2. Based on the published accuracy of the total station and standard error propagation, errors for the cliff face velocities are estimated at 0.014 ma^{-1} and applied to all calculations. Summer 2004-2005 velocities in the cliff-parallel direction averaged 2.13 ma^{-1} while flow perpendicular to the cliff averaged 2.04 ma^{-1}. During the following winter velocities averaged 1.98 ma^{-1} (cliff-parallel) and 2.27 ma^{-1} (cliff-perpendicular) (Table 4). A calving event at Cliff Site 1 over the winter of 2006 destroyed four of the ten stakes in the array.

Table 4: Velocities at Cliff Sites 1 and 2 for summer 2004-2005 and winter 2005.

Cliff Site 1					
Stake Number	Cliff Height	Summer 2004-2005		Winter 2005	
		Cliff-parallel	Cliff-perpendicular	Cliff-parallel	Cliff-perpendicular
1	24.32 m	2.11 ma^{-1}	2.24 ma^{-1}	--	--
2	21.21	2.17	2.25	1.98 ma^{-1}	2.29 ma^{-1}
3	18.33	1.85	2.74	2.03	2.05
4	15.19	2.15	2.27	2.03	2.45
5	12.19	2.09	2.31	0.72	1.48
6	9.19	2.52	1.59	1.96	2.25
7	6.32	2.45	1.53	1.91	2.30
8	5.00	1.82	1.98	--	--
9	4.51	1.94	1.69	--	--
Cliff Site 2					
Stake Number	Cliff Height	Summer 2004-2005		Winter 2005	
		Cliff-parallel	Cliff-perpendicular	Cliff-parallel	Cliff-perpendicular
1	33.44 m	2.26 ma^{-1}	2.03 ma^{-1}	1.70 ma^{-1}	2.30 ma^{-1}
2	30.47	2.00	2.28	1.76	2.37
3	27.54	1.97	2.26	1.76	2.35
4	24.00	2.82	2.21	--	--
5	21.67	1.99	2.36	1.81	2.40
6	18.59	1.98	2.36	1.82	2.22
7	15.72	1.73	2.38	1.82	2.64
8	12.70	1.87	2.21	1.76	2.15
9	10.00	1.79	2.40	--	--
10	7.05	1.55	1.96	--	--

At Cliff Site 2 summer velocities averaged 1.91 ma^{-1} (cliff-parallel) and 2.25 ma^{-1} (cliff-perpendicular) and winter velocities, 1.77 ma^{-1} and 2.35 ma^{-1} (Table 4). The data from Cliff Site 2 are more consistent than those at Cliff Site 1 and are considered more reliable. Summer cliff-parallel velocities at Cliff Site 2 increase with cliff height, as expected (Figure 32) and agree with previous work (Hubbard et al., *pers comm*. 2005). Cliff-perpendicular velocities are largely consistent from the top to the bottom of the cliff. Only stakes 1 (very top) and 10 (very bottom) show significantly lower velocities (Figure 32).

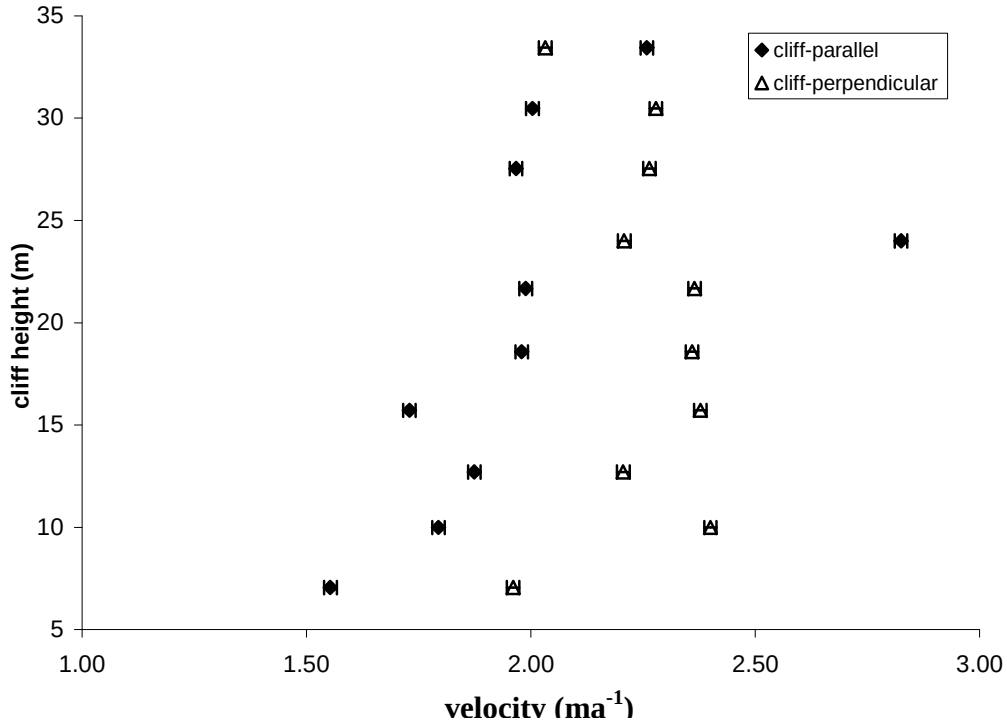

Figure 32: Cliff-parallel and cliff-perpendicular velocities measured at Cliff Site 2 during Summer 2004-2005.

Winter velocities at Cliff Site 2 do not show the same pattern. Cliff-parallel velocities only range 0.10 ma^{-1} from top to bottom of the cliff and cliff-perpendicular velocities do not show any significant trends.

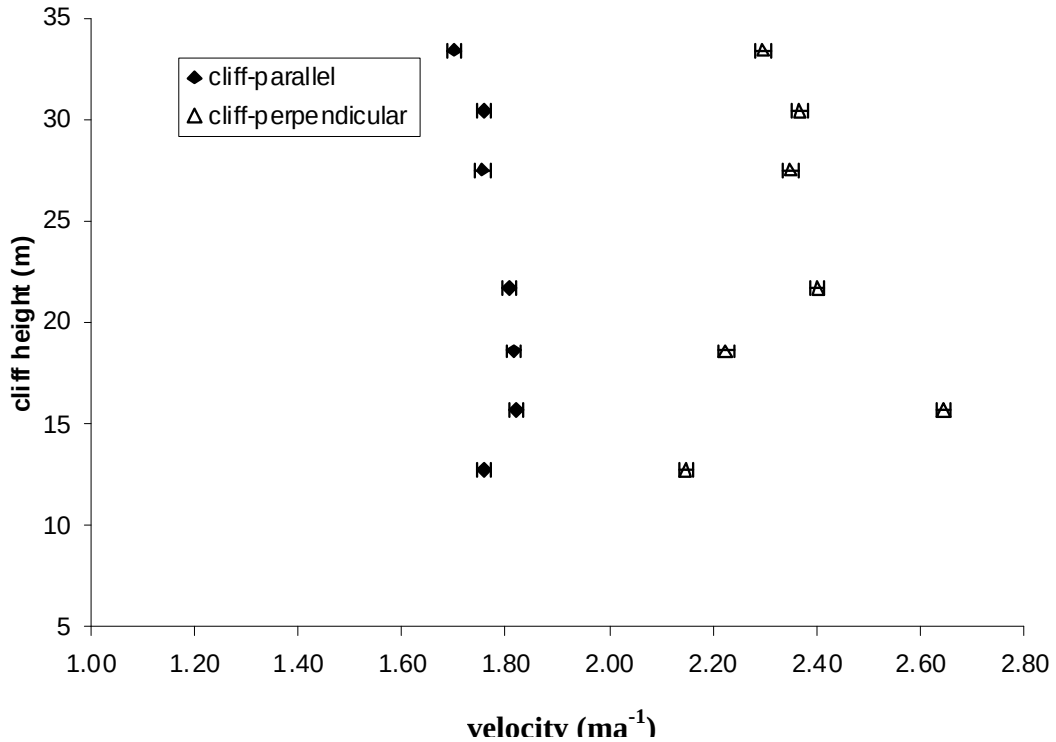

Figure 33: Cliff-parallel and cliff-perpendicular velocities measured at Cliff Site 2 during winter 2005.

Summer velocities are more erratic at Cliff Site 1 and a pattern of increasing velocity with cliff height does not emerge. The data do show a pattern in which increase in one component is accompanied by decrease in the other (Figure 34). This could be due to data processing rather than a physical process. Winter velocities are consistent with those at Cliff Site 2, however. Both velocity components show little variation across the cliff face with the exception of one stake, which is interpreted as an anomaly (Figure 35).

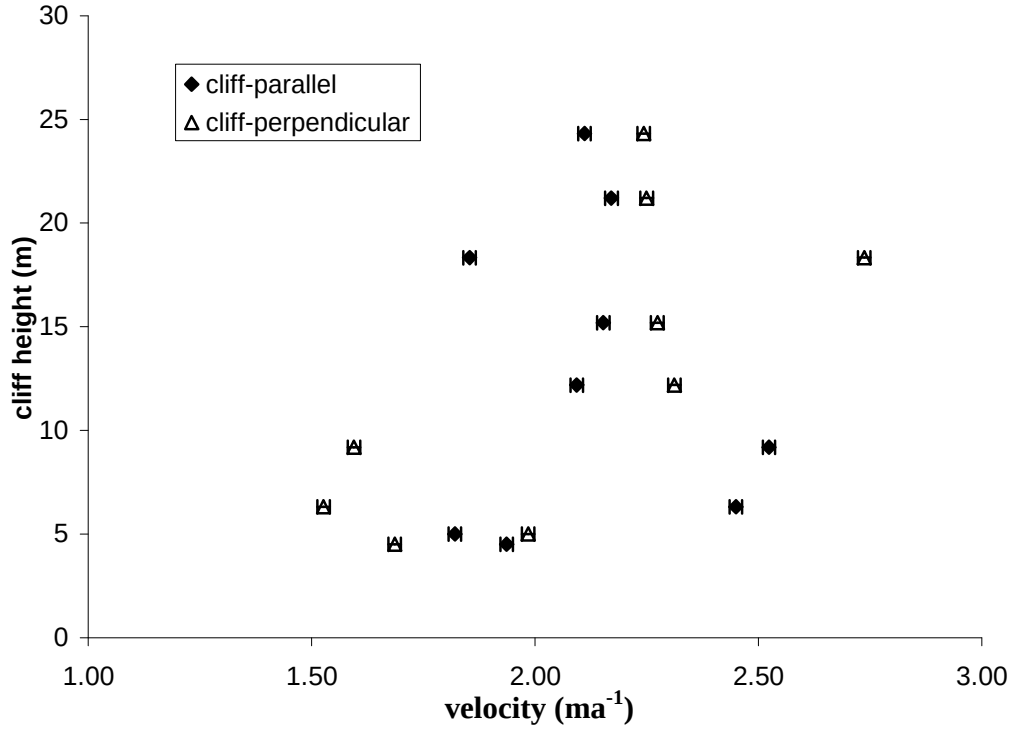

Figure 34: Velocities measured at Cliff Site 1 for the summer of 2004-2005.

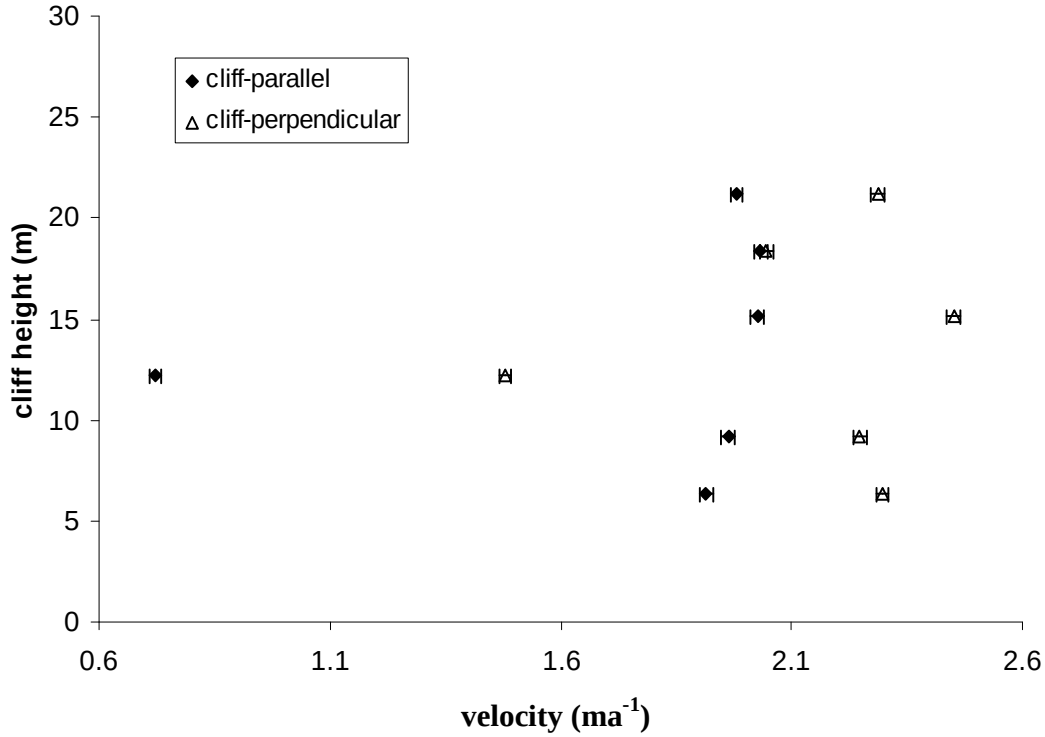

Figure 35: Winter 2005 velocities measured at Cliff Site 1

Ablation values at both sites are similar and show a significant increase of ablation towards the base of the cliffs. During the summer months, ablation ranged from 40 cm to over 100 cm at the base of the cliff. Total ablation decreased over the winter of 2005 from an average of 77 cm (Cliff Site 1) and 65 cm (Cliff Site 2) to 53 cm and 45 cm, respectively. The majority of the change is accounted for in the three lowest stakes. At Cliff Site 2, ablation at stake 9 decreased by 74 cm from 113 cm to 39 cm, while ablation at stake 3 only decreased a total of 13 cm from 49cm to 36 cm (Figure 36).

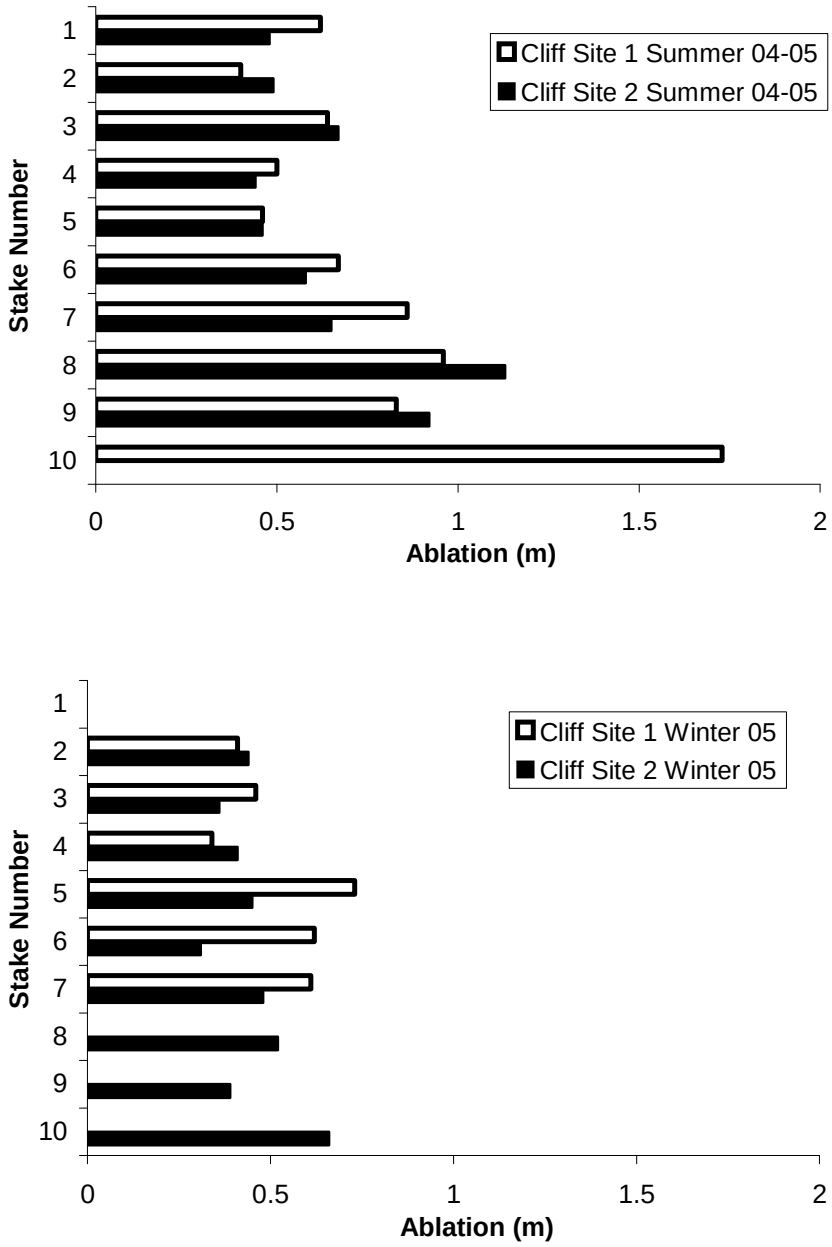

Figure 36: Ablation for both cliff sites for summer of 2004-2005 (top) and winter 2005 (bottom). Values for Cliff Site 1 are represented by hollow bars. Both sites lost stakes over the winter season.

Ice flow and ablation on the cliff determine the changing profile of the cliff face. The data from this project show two significant trends in regard to cliff profile development. In general cliff-perpendicular ice flow decreases with height in the cliff profile, which taken alone creates an overhanging cliff profile. Ablation is highest at the base of the cliff with values as high as 173 cm over only 56 days of the summer season. In the summer season ablation outpaces ice flow resulting in a net retreat of the cliff margin. However in the winter season there was a net advance of the cliff margin (Figure 37).

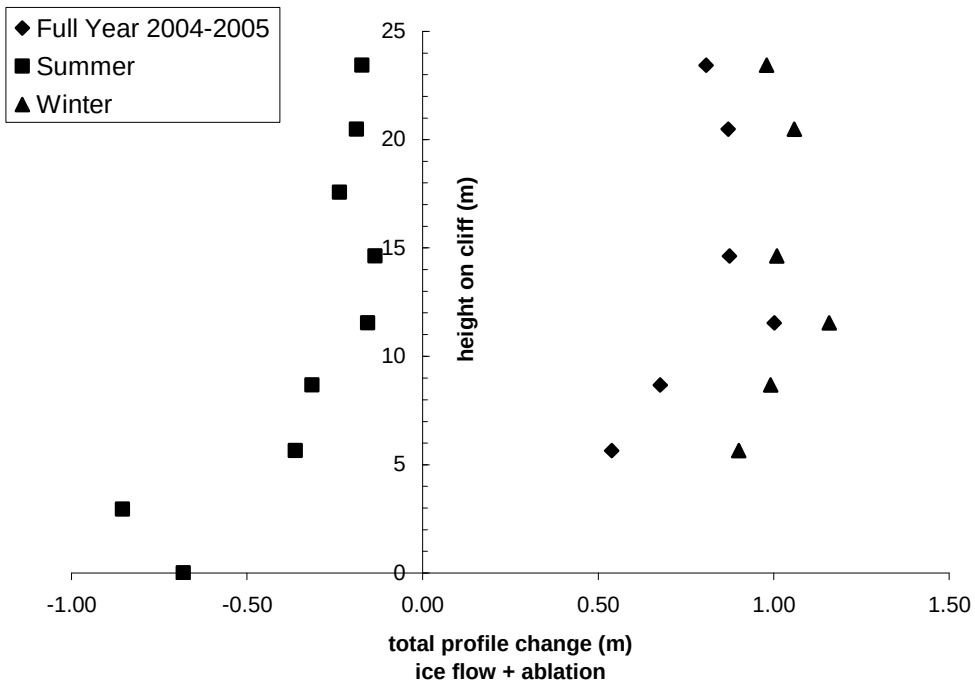

Figure 37: Cliff profile change at Cliff Site 2 showing summer, winter, and total year profile change.

There is no evidence either supporting or refuting the theories of Chinn and Hughes that link calving polar ice cliffs to isoclinal folding of terminal ice or deformation shear banding. However, over the full course of the 2004-2005 season at Site 2 there was a net advance of the cliff and the combined effects of ice flow and ablation result in an overhanging cliff that may be analogous to the undercutting observed in tidewater calving. This suggests agreement with the theories of tidewater calving advanced by Hanson and Hooke (2000) and Kirkbride and Warren (1997) which relate calving rate to factors such as wave-action undercutting and submarine melting. At Taylor Glacier the mechanism of ice removal at the base is a combination of ice flow and ablation that may be driven by differential long-wave energy radiation but the results are the same: an overhanging unstable cliff profile and calving.

Chapter 5: Conclusion

The local flow regime within 25 meters of the terminus of Taylor Glacier is consistent with simple shear. Surface velocities near the terminus show increasing down-glacier (cliff-parallel) velocity with distance from the cliff edge. The data show little to no variation of cliffward velocity with distance from the cliff edge. Strain rate calculations based on these velocities are inconclusive but may be consistent with a stress regime of simple shear. Principle strain rates may also be consistent with observed fracture patters particularly during the summer months

Maps of fractures within 25 meters of the terminus show a network of fractures oriented at oblique angles to the cliff edge that are also consistent with a stress regime of simple shear. In addition, fractures are more cliff-parallel nearer to the cliff edge. Finally, in areas where calving events have occurred, fractures may respond to changes in stress after the calving event.

Ice flow and ablation on the near-vertical cliff face may undercut the cliff leading to an overhanging cliff profile. This could lead to an unstable cliff and ultimately the observed local calving events on Taylor Glacier.

I suggest that surface ice flow establishes a stress regime consistent with simple shear, which leads to the formation of fractures oblique to the cliff edge. As these fractures approach the cliff edge through normal glacier flow, the ice is increasingly under the influence of local stresses of the cliff and the fractures open in more cliff-parallel orientations. Ice flow and ablation on the near-vertical cliff face cause local instability of the cliff. The strain caused by the overhanging cliff face is

accommodated preferentially across the previously formed fractures at the surface and calving events may eventually rupture along these fractures.

Future Work

The data collected for this project are incomplete. Errors associated with both optical and GPS measurements are too large to accurately calculate strain on Taylor Glacier. Increasing the duration of the study could improve strain errors.

The strain calculations in this project were fundamentally flawed by a lack of accuracy that is unlikely to improve significantly with a change in field methods. An alternative way to study the stresses and strain at the terminus of Taylor Glacier would be to conduct a detailed fracture analysis. Results from this project suggest near-cliff fractures react to ice-flow patterns from the main body of the glacier as well as local effects of cliff-induced stresses. A detailed study of these fractures would be an easy and simple way to study stress and strain at the cliff.

Part of the motivation for this project was to compare dry calving in the McMurdo Dry Valleys to tidewater calving in temperate regions. The portion of Taylor Glacier that calves into the perennially frozen Lake Bonney may be the closest analogue to tidewater calving on the glacier and should be explored. The heavily crevassed area of Taylor Glacier where it flows into Lake Bonney is more accessible than its tidewater analogues and the slow ice velocities and frozen lake slow the calving process. There are locations on the glacier where internal structure and strain can be measured across dirty layers in the profile of the calving terminus without cutting or tunneling.

References

Benn, D. I., and Evans, D. J. A., 1998, Glaciers & Glaciation: London, Arnold, 624 p.

Chinn, T. J. H., 1985, Structure and equilibrium of the Dry Valleys glaciers: New Zealand Antarctic record, v. 6, p. 73-88.

-, 1987, Accelerated ablation at a glacier ice-cliff margin, Dry Valleys, Antarctica: Arctic and Alpine Research, v. 19, no. 1, p. 71-80.

-, 1989, Single folds at the margins of dry-based glaciers as indicators of a glacial advance: Annals of Glaciology, v. 12, p. 23-30.

-, 1991, Polar Glacier margin and debris features, *in* Memorie della Societa Geologica Italiana, Sienna, Italy, p. 25-44.

Conway, H., Cuffey, K. M., Grades, A. M., Hallet, B., Raymond, C. F., and Sletten, R., 1996, Basal processes at subreezing temperatures: Meserve Glacier revisited: Antarctic Journal of the United States, v. 31, no. 2, p. 67-68.

Cuffey, K. M., Conway, H., Gades, A. M., Hallet, B., Lorrain, R., Severinghaus, J. P., Steig, E. J., Vaughn, B., and White, J. W. C., 2000, Entrainment at cold glacier beds: Geology, v. 28, no. 4, p. 351-354.

Doran, P. T., McKay, C. P., Clow, G. D., Dana, G. L., Fountain, A. G., Nylen, T., and Lyons, B. W., 2002, Valley floor climate observations from the McMurdo dry valleys, Antarctica, 1986-2000: Journal of Geophysical Research, v. 107, no. D24, p. 13-1 -13-12.

Evans, D. J. A., 1989, Apron entrainment at the margins of sub-polar glaciers, north-west Ellesmere Island, Canadian High Arctic: Journal of Glaciology, v. 35, no. 121, p. 317-324.

Fitzsimons, S. J., 1999, Structure and strength of basal ice and substrate of a dry-based glacier:evidence for substrate deformation at sub-freezing temperatures: Annals of Glaciology, v. 28, p. 236-240.

Fountain, A. G., Lyons, W. B., Burkins, M., B., Dana, G. L., Doran, P. T., Lewis, K. J., McKnight, D. M., Moorhead, D. L., Parsons, A. N., Priscu, J. C., Wall, D. H., Wharton Jr., R. A., and Virginia, R. A., 1999, Physical controls on the Taylor Valley ecosystem, Antarctica: Bioscience, v. 49, no. 12, p. 961-971.

Goldthwait, R. P., 1960, Study of Ice Cliff in Nunatarssuaq, Greenland: U.S. Army Snow and Ice Permafrost Research Establishment; Corps of Engineers, 39.

-, 1961, Regimen of an Ice Cliff on land in Northwest Greenland, *in* Norden, ed., Physical Geography of Greenland, International Geopgraphical Congress, 19th, Symposium SD 2: Copenhagen, Denmark, Kongelige Danske Geografiske Selskab.

Hanson, B., and Hooke, R. L., 2000, Glacier calving: a numerical model of forces in the calving-speed/ water-depth relation: Journal of Glaciology, v. 46, no. 153, p. 188-196.

Holdsworth, G., 1969, Structural Glaciology of Meserve Glacier: Antarctic Journal of the United States, v. 4, no. 4, p. 126-128.

-, 1974, Meserve Glacier Wright Valley, Antarctica: Part 1, Basal Processes: Ohio State University, Institute of Polar Studies, Report no. 37.

Hubbard, B., Hubbard, A., Lawson, W., and Andreson, B., *pers comm*. 2005, Relative Softness of clean glacier ice and debris-rich basal ice: Measurement and modelling at Taylor Glacier, Antarctica.
Hughes, T., 1989a, Bending Shear: The rate-controlling mechanism for calving ice walls: Annals of Glaciology, v. 35, no. 120, p. 260-266.
-, 1989b, Calving ice walls: Annals of Glaciology, v. 12, p. 74-79.
Hughes, T., and Fastook, J., 1997, The relationship between calving rates, ice velocities and water depths.: Byrd Polar Research Center, The Ohio State University, 15.
Johnston, R., 2004, Channel morphology and surface energy balance on Taylor Glacier, Taylor Valley, Antarctica [Master's thesis]: Portland State University, 113 p.
Johnston, R., Fountain, A. G., and Nylen, T., 2005, Meltwater production in channels on Taylor Glacier, McMurdo Dry Valleys, Antarctica, and their implication for water runoff.: Annals of Glaciology, v. 40, p. 1-7.
Kirkebride, M. P., and Warren, C. R., 1997, Calving processes at a grounded ice cliff: Annals of Glaciology, v. 24, p. 116-121.
Lewis, K. J., Fountain, A. G., and Dana, G. L., 1999, How important is teminus cliff melt?: a study of the Canada Glacier terminus, Taylor Valley, Antarctica: Global and Planetary Change, v. 22, p. 105-115.
Meier, M. F., 1997, Calving Glaciers: Report of a Workshop February 28 - March 2, 1997, *in* Van der Veen, C. J., ed., BPRC Report No. 15: Columbus, Ohio, Byrd Polar Research Center, The Ohio State University, p. 194.
Nylen, T. H., Fountain, A. G., and Doran, P. T., 2004, Climatology of katabatic winds in the McMurdo dry valleys, southern Victoria Land, Antarctica: Journal of Geophysical Research, v. 109, no. D03114.
Paterson, W. S. B., 1994, The Physics of Glaciers: Oxford, Butterworth Heinmann.
Robinson, P. H., 1984, Ice dynamics and thermal regime of Taylor Glacier South Victoria Land, Antarctica: Journal of Glaciology, v. 30, no. 105, p. 153-160.
Taylor, John R. 1997, An introduction to error analysis: the study of uncertainties in physical measurement. University Science books, Sausalito California, 327p.
Van der Veen, C. J., 1996, Tidewater Calving: Journal of Glaciology, v. 42, no. 141, p. 375-385.
-, 1997, Calving Glaciers: Report of a Workshop February 28 - March 2, 1997: Byrd Polar Research Center, The Ohio State University.
-, 2002, Calving Glaciers: Progress in Physical Geography, v. 26, no. 1, p. 96-122.